

# GENERATING SYNTHETIC MIXED-TYPE LONGITUDINAL ELECTRONIC HEALTH RECORDS FOR ARTIFICIAL INTELLIGENT APPLICATIONS

Jin Li<sup>†‡</sup>, Benjamin J. Cairns<sup>‡</sup>, Jingsong Li<sup>†\*</sup>, Tingting Zhu<sup>‡\*</sup>

<sup>†</sup>Zhejiang University, <sup>‡</sup>University of Oxford

{jin.li, tingting.zhu}@eng.ox.ac.uk, ben.cairns@ndph.ox.ac.uk, ljs@zju.edu.cn

## ABSTRACT

The recent availability of electronic health records (EHRs) have provided enormous opportunities to develop artificial intelligence (AI) algorithms. However, patient privacy has become a major concern that limits data sharing across hospital settings and subsequently hinders the advances in AI. *Synthetic data*, which benefits from the development and proliferation of generative models, has served as a promising substitute for real patient EHR data. However, the current generative models are limited as they only generate *single type* of clinical data, i.e., either continuous-valued or discrete-valued. In this paper, we propose a generative adversarial network (GAN) entitled EHR-M-GAN which synthesizes *mixed-type* timeseries EHR data. EHR-M-GAN is capable of capturing the multidimensional, heterogeneous, and correlated temporal dynamics in patient trajectories. We have validated EHR-M-GAN on three publicly-available intensive care unit databases with records from a total of 141,488 unique patients, and performed privacy risk evaluation of the proposed model. EHR-M-GAN has demonstrated its superiority in performance over state-of-the-art benchmarks for synthesizing clinical timeseries with high fidelity. Notably, prediction models for outcomes of intensive care performed significantly better when training data was augmented with the addition of EHR-M-GAN-generated timeseries. EHR-M-GAN may have use in developing AI algorithms in resource-limited settings, lowering the barrier for data acquisition while preserving patient privacy.

## 1 INTRODUCTION

The past decade has witnessed ground-breaking advancements been made in computational health, owing to the explosion of medical data, such as electronic health records (EHRs) (Artzi *et al.*, 2020; Raket *et al.*, 2020; Menger *et al.*, 2019). The secondary uses of EHRs give rise to research in a wide range of varieties, especially machine learning (ML)-based digital health solutions for improving the delivery of care (Wilkinson *et al.*, 2020; Watson *et al.*, 2019; Futoma *et al.*, 2020; Esteva *et al.*, 2021; Rajkomar *et al.*, 2019). However, in practice, the benefits of data-driven research are limited to healthcare organizations (HCOs) who possess the data (Wirth *et al.*, 2021; Dinov, 2016). Due to concerns about patient privacy, HCO stakeholders are reluctant to share patient data (Miotto *et al.*, 2018; Kim *et al.*, 2021; Simon *et al.*, 2019). Access to clinical data is often restricted, or can be prohibitively expensive to obtain, meaning that ML in biomedical research lags behind other areas in AI.

To accelerate the progress of developing AI methods in medicine, one promising alternative is for the data holder to create *synthetic* yet realistic data (Jordon *et al.*, 2018; Frid-Adar *et al.*, 2018). By avoiding “one-to-one” mapping to the genuine data compared with data anonymization, synthetic data offers a solution to circumvent the issue of privacy, while the correlations in the original data distributions are preserved for downstream AI applications. There have been successes in the literature using synthetic data to improve AI models where otherwise not possible due to limited availability of resources (Jordon *et al.*, 2020; Chen *et al.*, 2021; Tucker *et al.*, 2020; El Emam *et al.*, 2021). For

\*Corresponding authors.

---

example, large-scale data sharing programs have been demanded for advancing studies related to COVID-19, such as in National COVID Cohort Collaborative (N3C) (N3C., 2021), and Clinical Practice Research Datalink (CPRD) database in the UK (CPRD., 2021).

The availability of data synthesis facilitates the development of data-driven clinical models in research community for healthcare. However, some of the methods for generating synthetic patient EHRs rely heavily upon hand-crafted rules or clinical expertise (McLachlan *et al.*, 2016; Lombardo & Moniz, 2008). For example, McLachlan *et al.* (McLachlan *et al.*, 2016) proposed to generate synthetic EHRs by formalizing the clinical practice guidelines into a state transition machine (STM), with the whole process being domain knowledge-intensive. In addition, since these methods can only handle data with low dimensionality (and are typically disease-specific), the general utility of these methods is severely limited. Recent advances in generative adversarial networks (GANs) (Goodfellow *et al.*, 2014) and their variants offer more efficacious means to generate multidimensional, high-fidelity data with complex correlations for many different applications (Kearney *et al.*, 2020; Yang *et al.*, 2018; Marouf *et al.*, 2020). Furthermore, owing to their flexible tuning techniques, GAN models can better generate samples of anomalous or sparse events, mitigating the issue of the rarity which potentially leads to bias during training downstream ML models (Zhou *et al.*, 2020; Schlegl *et al.*, 2019).

EHRs are sets of digital patient-centered records collected over time, thereby recording patient health status and care *trajectories* during the hospitalization. Recent research has aimed to use this information to generate clinical *timeseries* which capture the character of these *trajectories* (Esteban *et al.*, 2017; Lee *et al.*, 2020; Zhang *et al.*, 2021; Kiyasseh *et al.*, 2020). In this study, we focus on generating timeseries in critical care, specifically in intensive care units (ICUs) where patient information are fully digitized. In the high-paced ICUs, various measurements and complex signals are recorded as *mixed-type* data for critically ill patients undergoing intensive monitoring (Sanchez-Pinto *et al.*, 2018; Shillan *et al.*, 2019) (see Fig. 1 for data extraction). Typically, two types of data are observed: (1) the *continuous-valued* physiological signals, such as heart rate (HR), oxygen saturation (SpO<sub>2</sub>), and measurements from blood gas tests; (2) the *discretized-valued* medical intervention data that change over time, including the usage of therapeutic devices or intravenous medications. Also, these mixed-type clinical timeseries are highly correlated (Yu *et al.*, 2019; Ghassemi *et al.*, 2017; Wang *et al.*, 2019). For example, the medications prescribed to patients rely heavily on measurements of their physiological status in the ICU. Meanwhile, the efficacy of the medical treatments, in turn, can critically affect the patient's physiological condition.

While *mixed-type* data can provide a rich environment for developing ML algorithms for assisting decision-making in critical care, they also impose complexity in creating generative models. As a result, most recent research has investigated how to synthesize the longitudinal data of different types separately, i.e., *with a focus only on continuous* or *only on discrete timeseries* (Yoon *et al.*, 2019; Lee *et al.*, 2020; Yu *et al.*, 2017). GANs have not previously been applied to address the issue in the mixed-data setting. Therefore for the first time, we propose a GAN for synthesizing mixed-type longitudinal EHR data (denoted as EHR-M-GAN thereafter). Patient trajectories with high-dimensionality and heterogeneous data type (both continuous-valued and discrete-valued timeseries) are generated while the underlying temporal dependencies are captured.

The main contributions of our work are as follows:

1. A novel GAN model entitled EHR-M-GAN is proposed for generating mixed-type multivariate EHR timeseries with high fidelity. EHR-M-GAN first maps data from different observational spaces into a reversible, lower-dimensional, shared latent space through a *dual variational autoencoder* (dual-VAE). Then, a sequentially coupled generator that is built upon a *coupled recurrent network* (CRN) is employed to capture the correlated temporal dynamics of the mixed-type data. In addition, a conditional version of our model — EHR-M-GAN<sub>cond</sub> — is also implemented, which is capable of synthesizing condition-specific EHR patient data, such as those result in *ICU mortality* or *hospital readmission*. The code of our proposed work is publicly available on GitHub<sup>1</sup>.
2. Evaluations are performed based on three publicly available ICU datasets: MIMIC-III (Johnson *et al.*, 2016), eICU (Pollard *et al.*, 2018) and HiRID (Yèche *et al.*, 2021) from a total of 141,488 patients. Standardized preprocessing pipelines are applied for the three ICU datasets to provide

---

<sup>1</sup><https://github.com/jli0117/ehrMGAN>

---

generalizable machine learning benchmarks. The code for the end-to-end preprocessing pipelines is also available on GitHub<sup>2</sup>.

3. Our EHR-M-GAN outperforms the state-of-the-art benchmarks on a diverse spectrum of evaluation metrics. When compared to real EHR data, both qualitative and quantitative metrics are used to assess the representativeness of the mixed-type data and their inter-dependencies. We further demonstrate the advantages offered by EHR-M-GAN in augmenting clinical timeseries for downstream tasks under various clinical scenarios.
4. In the evaluation of privacy risks, we perform an empirical analysis on EHR-M-GAN based on membership inference attack (Shokri *et al.*, 2017). We then further evaluate the performance of EHR-M-GAN under the framework of differential privacy for its application in downstream task (Dwork, 2006).

## 2 METHODS

In this section, we first formulate the problem based on the *mixed-type* temporal EHR data and its corresponding mathematical notation. Then the proposed EHR-M-GAN model is introduced in details.

### 2.1 PROBLEM FORMULATION

The longitudinal patient EHR dataset is denoted as  $\mathcal{D} = \{(\mathbf{x}_{i,1:T_i})\}_{i=1}^N$ , with each record (e.g., individual patient) being indexed by  $i \in \{1, 2, \dots, N\}$ . Here we consider the  $i$ -th instance tuple  $\mathbf{x}_{i,1:T_i} = \{\mathbf{x}_{i,1:T_i}^C, \mathbf{x}_{i,1:T_i}^D\}$  consists of two components (i.e., two types of data). Let  $\mathbf{x}_{i,1:T_i}^C \in \mathbb{R}^{|J|}$  denote the  $|J|$ -dimensional continuous-valued timeseries, such as physiological signals from real-time bedside monitors. And  $\mathbf{x}_{i,1:T_i}^D \in \mathbb{Z}^{|K|}$  denotes the  $|K|$ -dimensional discrete-valued timeseries, such as life-support interventions with the categorical value indicate its status (presence or absence).

### 2.2 PROPOSED MODEL

The preliminary for GANs and conditional GANs can be found in Supplementary materials (See Section S.1.A). We factorize EHR-M-GAN into two key components (see Network architecture in Fig. 1): (1) a *dual-VAE* framework for learning the shared latent space representations; (2) an RNN-based *sequentially coupled generator* and its corresponding sequence discriminators. As shown in Fig. 1, during the *pretrain* stage, two types of temporal trajectories are first jointly mapped into a shared latent space (first component). Then, the *sequentially coupled generator* in EHR-M-GAN (second component) produces the synthetic latent representations, which further can be recovered into features in the observational space by the pretrained decoders in the *dual-VAE*. Finally, the adversarial loss is provided based on discriminative results and backpropagated to update the network. The following sections discuss them in turn.

#### 2.2.1 DUAL-VAE PRETRAINING FOR SHARED LATENT SPACE REPRESENTATIONS

One prior of successfully training EHR-M-GAN to generate reversible latent codes is to meet the assumption that both  $\mathbf{x}_{i,1:T_i}^C$  and  $\mathbf{x}_{i,1:T_i}^D$  can be encoded into the *same* latent space  $\mathcal{H}^S \subset \mathbb{R}^{|S|}$  for the patient indexed with  $i$ , where  $|S|$  denotes its spatial dimension. For the sake of simplicity, the subscripts  $i$  are omitted throughout most of the paper. To achieve this, we propose to use a dual-VAE framework to encode both continuous and discrete multivariate timeseries into dense representations within  $\mathcal{H}^S$  based on multiple constraints. We found VAE preferable to vanilla autoencoder in our case, considering that (1) the KL regularization in VAE strengthens the learning of the compressed latent representations, which further narrow the domain gap for mixed-type features (Wan *et al.*, 2020); (2) VAE can be easily extended to the conditional learning scenario in EHR-M-GAN<sub>cond</sub>.

Fig. S1 (see Section S.1.B in Supplementary materials) diagrams the details of the proposed *dual-VAE* framework for learning the shared latent representations. We start with training two encoders, i.e.,  $Enc^C: \phi_{\mathcal{T} \times \mathcal{X}^C} \rightarrow \phi_{\mathcal{T} \times \mathcal{H}^S}$  and  $Enc^D: \phi_{\mathcal{T} \times \mathcal{X}^D} \rightarrow \phi_{\mathcal{T} \times \mathcal{H}^S}$ , with the embedding functions:

$$\mathbf{z}_{1:T}^C = Enc^C(\mathbf{x}_{1:T}^C) \quad \mathbf{z}_{1:T}^D = Enc^D(\mathbf{x}_{1:T}^D) \quad (1)$$

---

<sup>2</sup>[https://github.com/jli0117/preprocessing\\_physionet](https://github.com/jli0117/preprocessing_physionet)

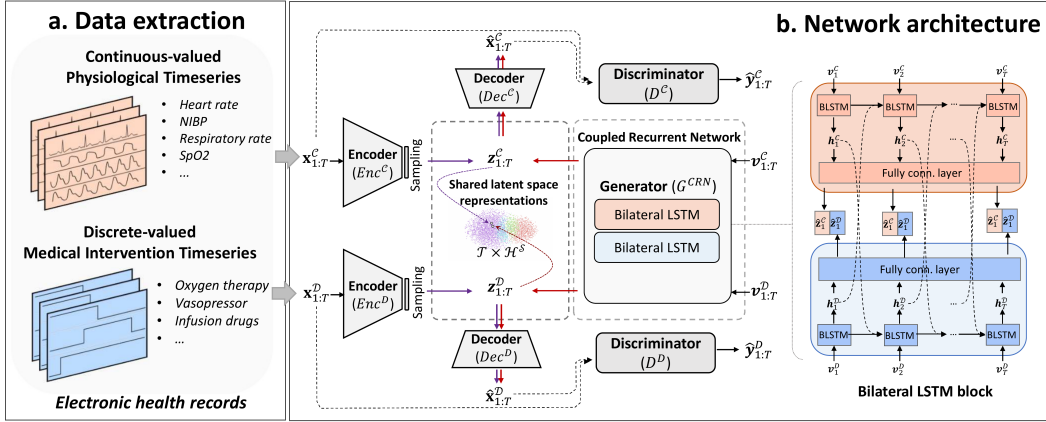


Figure 1: **Overall schematics.** **a. Data extraction.** Electronic health records (EHRs) data are routinely collected for patients in intensive care units (ICUs). Intensively monitored vital signals and laboratory measurements are recorded as continuous-valued timeseries, while the presence or absence of medical interventions is collected as discrete-valued timeseries during the ICU admission. **b. Network architecture.** EHR-M-GAN contains two key components. *Dual-VAE* is first pretrained for mapping heterogeneous data into shared latent representations (Step 1). Multiple objective loss constraints are used to bridge the domain gap, including ELBO loss, matching loss, contrastive loss, and semantic loss (for EHR-M-GAN<sub>cond</sub> only). Then, a *coupled recurrent network* (CRN) is established as the generator based on the parallel bilateral LSTM block (Step 2). After decoding the generated representations provided by CRN (Step 3), the adversarial loss is derived from the discriminators and backpropagated to update the network (Step 4).

After passing data from  $\mathcal{X}^C$  and  $\mathcal{X}^D$  through two encoders, a pair of embedding vectors  $(\mathbf{z}_{1:T}^C, \mathbf{z}_{1:T}^D)$  in the shared latent space  $\mathcal{H}^S$  can be obtained. Then the decoders for both domains  $Dec^C: \psi_{T \times \mathcal{H}^S} \rightarrow \psi_{T \times \mathcal{X}^C}$  and  $Dec^D: \psi_{T \times \mathcal{H}^S} \rightarrow \psi_{T \times \mathcal{X}^D}$  further reconstruct features based on the latent embeddings using mapping functions that operate in the opposite direction:

$$\tilde{\mathbf{x}}_{1:T}^C = Dec^C(\mathbf{z}_{1:T}^C) \quad \tilde{\mathbf{x}}_{1:T}^D = Dec^D(\mathbf{z}_{1:T}^D) \quad (2)$$

For the conditional extension in EHR-M-GAN<sub>cond</sub>, both encoders and decoders in the dual-VAE condition on the auxiliary (one-hot) labels from  $\mathcal{L}$ , to make the model better adapted to particular contexts. Also, to incentivize dual-VAE to better bridge the gap between domains of continuous-valued and discrete-valued timeseries, we enforce a weight-sharing constraint (Liu *et al.*, 2017; Liu & Tuzel, 2016) within specific layers of both the encoders pairs ( $Enc^C, Enc^D$ ), and the decoders pairs ( $Dec^C, Dec^D$ ). The weight-sharing constraint can extract and broadcast high-level concepts of the input features across domains of mixed-type data. The implementation details can be found in Supplementary materials (See Section S.1.B).

In the following subsections, we define multiple loss constraints for the optimization of *dual-VAE*, including *ELBO loss*, *Matching loss*, *Contrastive loss*, as well as *Semantic loss* for EHR-M-GAN<sub>cond</sub>. Intuitions and descriptions behind the objectives are discussed in turn.

**Evidence Lower Bound (ELBO).** We first incorporate the standard VAE loss, with the optimization objective as the evidence lower bound (ELBO). VAE holds the assumption of spherical Gaussian prior for the distribution of latent embeddings, where features can then be reconstructed by sampling from that space. We leverage the re-parameterization tricks to enable differentiable stochastic sampling and network optimization. For encoder and decoder in the dual-VAE for domain  $d \in \{C, D\}$ , the objective function is defined as:

$$\begin{aligned} \mathcal{L}_d^{\text{ELBO}} = & -\mathbb{E}_{q_\phi(\mathbf{z}|\mathbf{x})}[\log p_\psi(\mathbf{x}|\mathbf{z})] + \\ & \beta_{\text{KL}} D_{\text{KL}}(q_\phi(\mathbf{z}|\mathbf{x}) \| p_\psi(\mathbf{z})) \end{aligned} \quad (3)$$

where  $\mathbf{z} \sim Enc(\mathbf{x}) \triangleq q_\phi(\mathbf{z}|\mathbf{x})$ ,  $\tilde{\mathbf{x}} \sim Dec(\mathbf{z}) \triangleq p_\psi(\mathbf{x}|\mathbf{z})$ , and  $D_{\text{KL}}$  is the Kullback-Leibler divergence. The first term in Eq. (3) is the expected log likelihood term that penalizes the deviations

---

in reconstructing the inputs, while the second term of KL-divergence is the regularization imposed over the latent distribution from its Gaussian prior (normally chosen to be  $\mathcal{N}(\mathbf{0}, \mathbf{I})$ ).  $\beta_{\text{KL}}$  is the hyperparameter for balancing the weights between two terms.

**Matching loss.** Typically, representations derived from the *same* patient are assumed to capture the shared context. Therefore, embedding vectors  $(\mathbf{z}_{i,1:T_i}^{\mathcal{C}}, \mathbf{z}_{i,1:T_i}^{\mathcal{D}})$  in the shared latent space projected from the *same* patient  $i$ , are supposed to be positioned in close proximity (See Fig. S1 in Supplementary materials). Hence, the pairwise matching loss is incorporated to motivate the encoders to minimize the distance within the corresponding representation pairs. In the low-dimensional Euclidean space, we optimize the network by using the following objective:

$$\mathcal{L}^{\text{Match}} = \mathbb{E}_{\mathbf{z} \sim p_{\mathbf{z}}} \left[ \sum_{t \in \mathcal{T}} \|\mathbf{z}_t^{\mathcal{C}} - \mathbf{z}_t^{\mathcal{D}}\|^2 \right] \quad (4)$$

The pairwise matching loss achieve its optimal when the distance proxy  $\mathcal{L}^{\text{Match}}$  becomes zero.

**Contrastive loss.** On the flip side, pairwise reconstruction error (i.e., intra-correlations within one instance) measured by *matching loss* neglects the commonalities present across patients (inter-correlations of data) (Kiyasseh *et al.*, 2021). In order to guarantee sufficient bound for representation learning, we incorporate *contrastive loss* as another distance metric to capture the inter-correlations among the population.

Contrastive learning is a concept that has recently been popularized in self-supervised learning (SSL) and representation learning, which aims to capture intrinsic patterns from input data without human annotations. The core of contrastive learning is to encourage networks to attract positive pairs closer and repulse negative pairs apart in the latent space. In this study, we instantiate the contrastive loss via *NT-Xent*, which is proposed by Chen *et al.* in their work SimCLR (Chen *et al.*, 2020b). We define the corresponding auxiliary tasks for calculating the contrastive loss as — whether a set of representations transformed from the observational space belong to the *same* patient. And this leads to the corresponding positive pairs (true) and negative pairs (false).

For patient data of  $N$  records, we can obtain  $N$  pairs of latent representations from the encoders in *dual-VAE*. For patient indexed with  $i$ ,  $\mathbf{h}_i^{\mathcal{C}}$  and  $\mathbf{h}_i^{\mathcal{D}}$  denotes the embeddings derived from the continuous-valued and discrete-valued observational space, respectively. Due to the symmetric architecture of *dual-VAE*, here we use  $d$  and  $d'$  to represent one of each different domain, i.e.,  $d, d' \in \{\mathcal{C}, \mathcal{D}\}$  and  $d \neq d'$ . Therefore, the positive pairs for patient  $i$  can be referred as  $(i^d, i^{d'})$ , while the other  $2(N - 1)$  samples are regarded as negative pairs. Then the contrastive loss for a positive pair  $(i^d, i^{d'})$  is defined as:

$$\mathcal{L}_{i^d, i^{d'}}^{\text{Contra}} = -\log \frac{\exp(\text{sim}(\mathbf{h}_{i^d}, \mathbf{h}_{i^{d'}}) / \tau)}{\sum_{i^{dd'}=1}^{2N} \mathbb{1}_{[i^{dd'} \neq i^d]} \exp(\text{sim}(\mathbf{h}_{i^d}, \mathbf{h}_{i^{dd'}}) / \tau)} \quad (5)$$

where  $\text{sim}(u, v) = u^T v / \|u\| \|v\|$  denotes the cosine similarity between two vectors.  $\tau > 0$  denotes a temperature hyperparameter.  $\mathbb{1}_{[n \neq m]} \in \{0, 1\}$  is an indicator evaluating to 1 iff  $n \neq m$ . And  $i^{dd'} \in \{1, 2, \dots, 2N\}$  represents the index of latent embeddings from *both* data types. The final contrastive loss is computed across the total number of  $|i^d - i^{d'}| = N$  positive pairs for both  $(i^d, i^{d'})$  and  $(i^{d'}, i^d)$ , and is defined as:

$$\mathcal{L}^{\text{Contra}} = \frac{1}{2N} \sum_{i^d=1}^N \sum_{i^{d'}=1}^N [\mathcal{L}_{i^d, i^{d'}}^{\text{Contra}} + \mathcal{L}_{i^{d'}, i^d}^{\text{Contra}}] \quad (6)$$

**Semantic loss.** In EHR-M-GAN<sub>cond</sub>, semantic loss is imposed to better align patients with same labels (conditions) into the same latent space clusters. For example, if the label of *severe clinical deterioration* in the ICU is given for conditional data generation, the corresponding synthetic continuous-valued timeseries (e.g., severely deranged vital signs) is supposed to be strongly associated with the discrete-valued timeseries (e.g., intensive medical interventions) under the same label. For both domains, additional linear classifiers are trained to classify the latent embeddings based on their corresponding conditions in the observational space. We implement logistic regression as

the linear classifiers and calculate the cross entropy as the semantic losses for both domains. For  $d \in \{\mathcal{C}, \mathcal{D}\}$ , given the latent embedding vector  $\mathbf{z}^d$  and the conditional information vector  $\mathbf{y}$ :

$$\mathcal{L}_d^{\text{Class}} = \mathbb{E}_{\mathbf{z}^d \in \mathcal{H}^{\mathcal{S}}} \text{CE}(f_{\text{linear}}^d(\mathbf{z}^d), \mathbf{y}) \quad (7)$$

where  $f_{\text{linear}}^d$  denotes the linear classifier for the corresponding domain. And  $\text{CE} = -\sum_j y_j \log(\hat{y}_j)$ , ( $j = 1, 2, \dots, |L|$ ) denotes the cross entropy loss, where  $\hat{y}_j$  is the output of the linear classifier, and  $y_j$  is the ground truth label for class  $j$  in condition vector  $\mathbf{y}$ .

In summary, to train the *dual-VAE* for learning the shared latent space representation, the total objective function for  $d \in \{\mathcal{C}, \mathcal{D}\}$  is:

$$\mathcal{L}_d = \beta_0 \mathcal{L}_d^{\text{ELBO}} + \beta_1 \mathcal{L}^{\text{Match}} + \beta_2 \mathcal{L}^{\text{Contra}} \quad (8)$$

Under the conditional learning scenario of EHR-M-GAN<sub>cond</sub>, the total loss becomes:

$$\mathcal{L}_d = \beta_0 \mathcal{L}_d^{\text{ELBO}} + \beta_1 \mathcal{L}^{\text{Match}} + \beta_2 \mathcal{L}^{\text{Contra}} + \beta_3 \mathcal{L}_d^{\text{Class}} \quad (9)$$

where  $\beta_0, \beta_1, \beta_2$ , and  $\beta_3$  are scalar loss weights used to balance the loss terms.

### 2.2.2 SEQUENTIALLY COUPLED GENERATOR BASED ON CRN

The objective of EHR-M-GAN is to capture the dynamics in the mixed-type timeseries, which can be regarded as the composition of the spatial and temporal correlations. To this end, we propose the *sequentially coupled generator*, which is built based on the *coupled recurrent network (CRN)*. Specifically, a CRN comprises two *single recurrent networks (SRN)* (one for each type of the multivariate spatial timeseries, i.e., continuous or discrete-valued). In each SRN, LSTM network is introduced as the recurrent layer to preserve the temporal dependencies in the sequences. The description for the basic structure of SRN can be found in the Supplementary materials (see Section S.1.C). In the following section, we first discuss the structure of BLSTM in detail as an essential part of CRN, and then build the *sequentially coupled generator* based on CRN.

**Bilateral long short-term memory.** As shown in Fig. 1, two streams of BLSTM entangles with each other in a CRN, and are jointly trained to sequentially exploit the correlations between two types of trajectories. Given  $d, d' \in \{\mathcal{C}, \mathcal{D}\}$  in CRN, since two branches of BLSTM associated with the corresponding domains are symmetric, we present the mathematical expressions from the perspective of branch  $d$  as an example to illustrate the algorithm of BLSTM in details. Similar as the formulations in SRN (see Section S.1.C for the detailed description),  $\mathbf{v}_t^d$  and  $\mathbf{h}_t^d$  denotes the input vector and hidden state vector for domain  $d$  at time step  $t$ , respectively. An additional set of weights for introducing hidden states representations  $\mathbf{h}_t^{d'}$  from domain  $d'$  is included when updating the input gate  $\mathbf{i}_t^d$ , forget gate  $\mathbf{f}_t^d$ , output gate  $\mathbf{o}_t^d$ , and cell memory  $\tilde{\mathbf{c}}_t^d$ . The state transition functions for BLSTM are:

$$\begin{aligned} \mathbf{i}_t^d &= \sigma \left( \mathbf{W}_{idv} \mathbf{v}_t^d + \mathbf{W}_{idh^{d'}} \mathbf{h}_{t-1}^{d'} + \mathbf{W}_{idh^d} \mathbf{h}_{t-1}^d + \mathbf{b}_{id} \right) \\ \mathbf{f}_t^d &= \sigma \left( \mathbf{W}_{fdv} \mathbf{v}_t^d + \mathbf{W}_{fdh^{d'}} \mathbf{h}_{t-1}^{d'} + \mathbf{W}_{fdh^d} \mathbf{h}_{t-1}^d + \mathbf{b}_{fd} \right) \\ \mathbf{o}_t^d &= \sigma \left( \mathbf{W}_{odv} \mathbf{v}_t^d + \mathbf{W}_{odh^{d'}} \mathbf{h}_{t-1}^{d'} + \mathbf{W}_{odh^d} \mathbf{h}_{t-1}^d + \mathbf{b}_{od} \right) \\ \tilde{\mathbf{c}}_t^d &= \tanh \left( \mathbf{W}_{cdv} \mathbf{v}_t^d + \mathbf{W}_{cdh^{d'}} \mathbf{h}_{t-1}^{d'} + \mathbf{W}_{cdh^d} \mathbf{h}_{t-1}^d + \mathbf{b}_{cd} \right) \\ \mathbf{c}_t^d &= \mathbf{f}_t^d \odot \mathbf{c}_{t-1}^d + \mathbf{i}_t^d \odot \tilde{\mathbf{c}}_t^d \\ \mathbf{h}_t^d &= \mathbf{o}_t^d \odot \tanh(\mathbf{c}_t^d) \end{aligned} \quad (10)$$

The additional set of weights in BLSTM facilitates the model to intrinsically decide how much information it should pass through the gates from its counterpart. An illustration of the BLSTM cell can be found in the Supplementary materials (see Fig. S2).

**Coupled recurrent network.** The architecture of CRN consists of three layers: the *input layers*, the *recurrent layers*, and the *fully connected layers*. First, the random noise vectors  $\mathbf{v}_t^d$  and  $\mathbf{v}_t^{d'}$  for two domains are separately fed into the *input layers*. Then the *recurrent layers*  $f_{\text{rec}}$ , which are built based on BLSTM as suggested in Eq. (10), are used to recursively iterate hidden states from both branches.

---

Finally, the *fully connected layers*  $f_{\text{conn}}^d$  and  $f_{\text{conn}}^{d'}$  produce the generated latent vectors  $\hat{\mathbf{z}}_t^d$  and  $\hat{\mathbf{z}}_t^{d'}$  for the decoding stage in *dual-VAE*. At time step  $t$ , CRN can be formulated as:

$$\begin{aligned} (\mathbf{h}_t^d, \mathbf{h}_t^{d'}) &= f_{\text{rec}}((\mathbf{v}_t^d, \mathbf{v}_t^{d'}), (\mathbf{h}_{t-1}^d, \mathbf{h}_{t-1}^{d'})) \\ \hat{\mathbf{z}}_t^d &= f_{\text{conn}}^d(\mathbf{h}_t^d) \\ \hat{\mathbf{z}}_t^{d'} &= f_{\text{conn}}^{d'}(\mathbf{h}_t^{d'}) \end{aligned} \quad (11)$$

Note that the parameters are initialized independently within the two branches of the recurrent layers  $f_{\text{rec}}$  regardless of the coupled architecture of the network. With respect to EHR-M-GAN<sub>cond</sub>, the generator  $G^{\text{CRN}}$  generates synthetic latent embeddings conditioned on the auxiliary information  $\mathbf{y}$  (conditional labels  $\mathbf{y}$  are also incorporated during the pretrain stage for *dual-VAE*). In summary, heterogeneous timeseries that exhibits mutual influence are integrated into the parallelly coupled network architecture to leverage the shared information. By introducing BLSTM, two streams of the inputs in the generator are encouraged to “communicate” with each other. CRN is therefore capable of exploiting the interplay between mixed-type data that correlates over time.

### 2.2.3 JOINT TRAINING AND OPTIMIZATION

The overall architecture of EHR-M-GAN is shown in Fig. 1. In this section, we give a detailed description of the entire network’s structure and the optimization objective of the model. The steps for the training and optimization of EHR-M-GAN are as follows:

1. The *pretraining of dual-VAE*: First, a dual-VAE network which consists of a pair of encoders ( $Enc^{\mathcal{C}}, Enc^{\mathcal{D}}$ ) and decoders ( $Dec^{\mathcal{C}}, Dec^{\mathcal{D}}$ ) is pretrained. Based on multiple objective constraints in Eq. 8 (for EHR-M-GAN<sub>cond</sub> the objective function can be referred in Eq. 9), a shared latent space is learnt using *dual-VAE*, where the gap between the embedding representations ( $\mathbf{z}_{1:T}^{\mathcal{C}}, \mathbf{z}_{1:T}^{\mathcal{D}}$ ) from both domains is minimized.
2. The *generation of latent representations based on CRN*: Then, during the joint training stage, the *sequentially coupled generator* is built based on CRN with the internal transition functions iterating across the timesteps  $t \in \{1, 2, \dots, T\}$ . Therefore, the synthetic latent embedding representations ( $\hat{\mathbf{z}}_{1:T}^{\mathcal{C}}, \hat{\mathbf{z}}_{1:T}^{\mathcal{D}}$ ) for both types of data can be obtained.
3. The *decoding for the mixed-type timeseries*: Next, the generated latent embeddings ( $\hat{\mathbf{z}}_{1:T}^{\mathcal{C}}, \hat{\mathbf{z}}_{1:T}^{\mathcal{D}}$ ) are further fed into the pretrained decoders ( $Dec^{\mathcal{C}}, Dec^{\mathcal{D}}$ ) and decoded into the corresponding synthetic patient trajectories ( $\hat{\mathbf{x}}_{1:T}^{\mathcal{C}}, \hat{\mathbf{x}}_{1:T}^{\mathcal{D}}$ ) in the observational space.
4. The *adversarial loss update based on the discriminators*: Finally, the adversarial loss can be calculated from the LSTM network-based discriminators  $D^{\mathcal{C}}$  and  $D^{\mathcal{D}}$  by distinguishing between the real samples and synthetic timeseries.

Note that in the conditional version of EHR-M-GAN<sub>cond</sub>, the discriminators are also conditioned on the same auxiliary labels information as in the generator. The mathematical expressions for the min-max objectives in EHR-M-GAN and EHR-M-GAN<sub>cond</sub> are provided as follows:

$$\begin{aligned} \min_G \max_D V_{\text{EHR-M-GAN}} &= \mathbb{E}_{\mathbf{x} \sim p_{\mathbf{x}}} [\log D^{\mathcal{C}}(\mathbf{x}^{\mathcal{C}}) + \log D^{\mathcal{D}}(\mathbf{x}^{\mathcal{D}})] + \\ &\quad \mathbb{E}_{\mathbf{v} \sim p_{\mathbf{v}}} [\log(1 - D^{\mathcal{C}}(\hat{\mathbf{x}}^{\mathcal{C}})) + \log(1 - D^{\mathcal{D}}(\hat{\mathbf{x}}^{\mathcal{D}}))] \end{aligned} \quad (12)$$

$$\begin{aligned} \min_G \max_D V_{\text{EHR-M-GAN}_{\text{cond}}} &= \mathbb{E}_{\mathbf{y}, \mathbf{x} \sim p_{\mathbf{y}, \mathbf{x}}} [\log D^{\mathcal{C}}(\mathbf{x}^{\mathcal{C}} | \mathbf{y}) + \log D^{\mathcal{D}}(\mathbf{x}^{\mathcal{D}} | \mathbf{y})] + \\ &\quad \mathbb{E}_{\mathbf{y} \sim p_{\mathbf{y}}, \mathbf{v} \sim p_{\mathbf{v}}} [\log(1 - D^{\mathcal{C}}(\hat{\mathbf{x}}^{\mathcal{C}} | \mathbf{y})) + \log(1 - D^{\mathcal{D}}(\hat{\mathbf{x}}^{\mathcal{D}} | \mathbf{y}))] \end{aligned} \quad (13)$$

The pseudocodes for dual-VAE and EHR-M-GAN are provided in the Supplementary materials (see Section S.1.C).

---

### 3 DATA AND EVALUATION

#### 3.1 DATASET DESCRIPTION

The following three publicly accessible ICU datasets are used for evaluating the performance of EHR-M-GAN in generating the longitudinal EHR data:

- **MIMIC-III** (Medical Information Mart for Intensive Care) (Johnson *et al.*, 2016) — a freely accessible database that comprises de-identified EHRs associated with approximately 60,000 ICU admitted patients and 312 million observations to Beth Israel Deaconess Medical Center.
- **eICU** (eICU Collaborative Research Database) (Pollard *et al.*, 2018) — a multi-center critical care database containing data for over 200,000 admissions and 827 million observations to ICUs from 208 hospitals located throughout the United States.
- **HiRID** (High time-resolution ICU dataset) (Yèche *et al.*, 2021) — a high-resolution ICU dataset relating to more than 3 billion observations from almost 34,000 ICU patient admissions, monitored at the Department of Intensive Care Medicine, Bern University Hospital, Switzerland. .

All these critical care databases include vital sign measurements, laboratory tests, treatment information, survival records, and other routinely collected data from hospital EHR systems. From these clinical observations, we featurize the patient trajectories as the combination of continuous-valued physiological timeseries and discrete-valued medical intervention timeseries. Data are preprocessed following an open-source framework — MIMIC-Extract (Wang *et al.*, 2020). Details on data curation, including the cohort selection criteria, full list of features, and imputation method, are explained in Supplementary Materials (see S.2 Datasets). Overall, the summarising statistics of the finalised cohorts for three databases are shown in Table 1.

Table 1: **Summary of the cohorts after preprocessing on three critical care databases.** Number of patients and ICU admissions are provided for each dataset. Note that only the first ICU admission is selected for each patient. The dimension of the continuous- and discrete-valued data are provided. The conditional labels for training EHR-M-GAN<sub>cond</sub> and the corresponding counts for each class are also listed.

	Number of patients	Number of ICU admissions	Dimension of continuous-valued variables	Dimension of discrete-valued variables	Conditional labels	Counts
MIMIC-III	28,344	28,344	78	20	ICU mortality	1,870 (6.59%)
					Hospital mortality	911 (3.21%)
					30-day readmission	1,122 (3.95%)
					No 30-day readmission	24,441 (86.22%)
eICU	99,015	99,015	55	19	ICU mortality	4,500 (4.54%)
					Hospital mortality	3,291 (3.32%)
					Hospital discharge	91,224 (92.13%)
HiRID	14,129	14,129	50	39	ICU mortality	1,266 (8.96%)
					ICU discharge	12,963 (91.74%)

#### 3.2 BASELINES MODELS

We compare the performance of EHR-M-GAN with six state-of-the-art generative methods: For continuous-valued timeseries generation, benchmark GAN models include C-RNN-GAN (Mogren, 2016), R(C)GAN (Esteban *et al.*, 2017) and TimeGAN (Yoon *et al.*, 2019). For discrete-valued timeseries generation, medGAN (Choi *et al.*, 2017), seqGAN (Yu *et al.*, 2017) and DualAAE (Lee *et al.*, 2020) are used for comparison. For medGAN, we feed the flattened temporal sequence as the input since the model cannot produce timeseries data. Also, an **ablation study** is performed to assess the effectiveness of distinct modules integrated in the proposed work. More specifically, two main components in our model are considered: *dual-VAE* for learning the shared latent representations, and *sequentially coupled generator* for capturing the temporal dynamics in mixed-type data. As a result, multiple variants of EHR-M-GAN are tested:

---

- $\text{GAN}_{\text{VAE}}$ : It contains the simplified version of EHR-M-GAN, which combines a pair of pretrained VAE networks and GANs (one for each type of inputs). The architectures of loss-constrained *dual-VAE* and *sequentially coupled generator* are not included.
- $\text{GAN}_{\text{SL}}$ : In addition to  $\text{GAN}_{\text{VAE}}$ , it learns the shared latent space representations through *dual-VAE* by adding the corresponding loss functions.
- EHR-M-GAN: In addition to  $\text{GAN}_{\text{SL}}$ , it incorporates the *sequentially coupled generator* for the learning the correlated temporal dynamics in timeseries of different data types. This is the proposed full model.
- EHR-M-GAN<sub>cond</sub>: This version is implemented on the basis of conditional GAN (Mirza & Osindero, 2014), where the conditional inputs are fed into EHR-M-GAN to generate patients under specific labels.

Temporal trajectories **24 hours prior to patients' ICU endpoints** (discharge or death) are extracted. For training EHR-M-GAN<sub>cond</sub>, auxiliary information from the patient status is used as conditional input. For MIMIC-III dataset, the classes are (1) *ICU mortality*: patient died within the ICU; (2) *Hospital mortality*: patient discharged alive from the ICU, and died within the hospital; (3) *30-day readmission*: patient discharged alive from the hospital, and readmitted to the hospital within 30 days; (4) *No 30-day readmission*: patient discharged alive from the hospital, and had no readmission record to the hospital within 30 days. For eICU and HiRID datasets, the corresponding labels are also extracted based on the availability of the patient outcomes (see Table 1).

### 3.3 EVALUATION METRICS

Evaluating GAN models is a notoriously challenging task. Advantages and pitfalls of commonly used evaluation metrics for GANs are discussed in (Borji, 2021). In this work, we first individually assess the representativeness of the synthetic continuous-valued and discrete-valued timeseries. This includes measuring the distance between underlying data distributions (such as *Maximum mean discrepancy* and *Dimension-wise probability*), comparing the indistinguishability of the synthetic data to the true data (i.e., *Discriminative score*). Secondly, we assess our model by using a set of qualitative metrics (such as *Embedding visualisation*, *Patient trajectory plot* and *Pearson pairwise correlations*) for evaluating to which extent our model can reconstruct the interdependency between two types of data. Thirdly, we introduce data augmentation by incorporating synthesized EHR timeseries under various settings, and quantitatively assess the improvement provided by EHR-M-GAN in the *Downstream tasks* for medical intervention prediction in the ICU. Lastly, we measure the attribute of patient privacy-preserving of EHR-M-GAN under *Membership inference attack*. We also evaluate the performance of the same downstream tasks under *Differential privacy* guarantees.

## 4 RESULTS

### 4.1 MAXIMUM MEAN DISCREPANCY

To measure the similarity between the continuous-valued synthetic data and the real data, maximum mean discrepancy (MMD) is used. MMD can assess whether two samples, in our case, true data  $x$  and synthetic data  $x'$ , are from the same distributions. It can be expressed as the first-order moments, i.e., mean embeddings, of the two samples in a reproducing kernel Hilbert space (RKHS):  $k(x, x') = \sum_i \exp(-\|x - x'\|^2 / \sigma_i^2)$ . We follow the implementations in (Sutherland *et al.*, 2016) by using a sum of Gaussian kernel sets.

Table 2: **Maximum mean discrepancy (MMD) of continuous-valued synthetic data.** Lower values of MMD indicate models which can better learn the distribution of the real data.

	C-RNN-GAN	R(C)GAN	TimeGAN	$\text{GAN}_{\text{VAE}}$	$\text{GAN}_{\text{SL}}$	EHR-M-GAN	EHR-M-GAN <sub>cond</sub>
<b>MIMIC-III</b>	$1.038 \pm 0.013$	$0.971 \pm 0.029$	$0.694 \pm 0.025$	$0.926 \pm 0.038$	$0.745 \pm 0.040$	<b><math>0.692 \pm 0.034</math></b>	<b><math>0.604 \pm 0.027</math></b>
<b>eICU</b>	$1.139 \pm 0.023$	$1.106 \pm 0.042$	$0.672 \pm 0.038$	$0.842 \pm 0.029$	$0.670 \pm 0.034$	<b><math>0.651 \pm 0.026</math></b>	<b><math>0.540 \pm 0.018</math></b>
<b>HiRID</b>	$0.982 \pm 0.017$	$0.865 \pm 0.020$	$0.470 \pm 0.024$	$0.532 \pm 0.035$	$0.508 \pm 0.028$	<b><math>0.428 \pm 0.015</math></b>	<b><math>0.389 \pm 0.024</math></b>

As indicated in Table 2, EHR-M-GAN outperforms the state-of-the-art benchmarks among all three datasets in synthesizing continuous-valued timeseries. The conditional version — EHR-M-GAN<sub>cond</sub>

further boosts the performance of the model by leveraging the information of the condition-specific inputs. Furthermore, as shown in the ablation study, EHR-M-GAN and EHR-M-GAN<sub>cond</sub> produce smaller MMD values when compared to their variants. Using MIMIC-III as an example, compared with the basic model GAN<sub>VAE</sub>, by integrating the shared latent space learning using *dual-VAE* under multiple loss constraints, the performance of GAN<sub>SL</sub> significantly improves (GAN<sub>SL</sub> vs. GAN<sub>VAE</sub>, 0.745 to 0.926, *p*-value < 0.05 from *t*-test<sup>3</sup>). By further building the sequentially coupled generator based on BLSTMs and exploiting the information within mixed-type data, the MMD of EHR-M-GAN shows a nearly 24% improvement over GAN<sub>VAE</sub>.

#### 4.2 DIMENSION-WISE PROBABILITY

To evaluate the representativeness of the synthetic discrete-valued timeseries, the dimension-wise probability test is employed. As a sanity check, it investigates if the distribution across the spatial and temporal dimensions is matched between the real and synthetic data. Therefore, the Bernoulli success probability  $p \in [0, 1]$  is calculated over all feature dimensions for the discrete-valued timeseries, and is visualized through scatterplot.

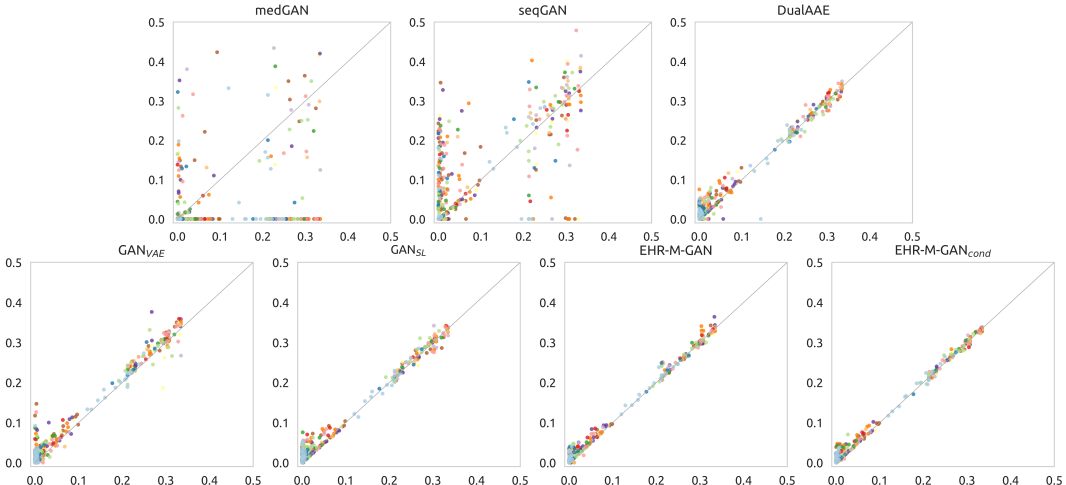


**Figure 2: Scatterplot of the dimension-wise probability test on MIMIC-III dataset.** The x-axis and y-axis represents the probability distribution for the real data and synthetic data with same sample size, respectively. Each dot represents a physiological measurement or treatment status at a particular time in the patient EHR data. Same color indicates same measurement or status (but with varying timestamps). The optimal performance appears along the diagonal line. Dimension-wise probability plot for eICU and HiRID dataset can be found in Supplementary materials (see S.3.A).

As shown in Fig. 2 (see Fig. S3 and S4 for more results on eICU and HiRID datasets), the optimal results are provided by EHR-M-GAN and EHR-M-GAN<sub>cond</sub>. The close-to-real probability distributions that appear along the diagonal line indicate the remarkable similarity between the real data and the synthetic data provided by our models. Similar to the results in MMD, the dimensional-wise distributions are better captured when modules such as *dual-VAE* and *sequentially coupled generator* are introduced in EHR-M-GAN.

Among all state-of-the-art benchmark models, DualAAE shows comparable results to EHR-M-GAN. While in contrast, skewed distributions are observed in medGAN versus the real data, as it is incapable to model the temporal correlations within timeseries. On the other hand, despite the well-known performance of SeqGAN in natural language generation (Yu *et al.*, 2017), it is not applicable in synthesizing sequential clinical EHRs.

Generating discrete-valued features are known to be problematic for traditional GANs. Due to their limitation in passing the gradients from the critic models, vanilla GANs cannot update their generators efficiently based on the adversarial loss (Yu *et al.*, 2017; Choi *et al.*, 2017). However, the result of

<sup>3</sup>Unpaired (two-sample) *t*-test with a significance level of 0.05 is used throughout the paper unless specified otherwise.

---

EHR-M-GAN shows its superiority in explicitly capturing each dimension of the discrete-valued sequences. EHR-M-GAN mitigates this problem by learning the shared latent representations using *dual-VAE*. Discrete-valued timeseries are encoded into a gradient-differentiable space for further optimizing the generators and thus solving the problem.

#### 4.3 DISCRIMINATIVE SCORE

For both continuous-valued and discrete-valued data, the discriminative score is measured as the accuracy of a discriminator trained post-hoc to separate real from generated samples. Synthetic data are generated with the same amount of the hold-out test set from the original data, and are labeled as *synthetic* and *real* correspondingly to train the binary classifier. We opt to implement the classifier as a single-layered Bi-directional Long Short-Term Memory (Bi-LSTM) model (i.e., *many-to-one*), to characterize the temporal correlations within the patient EHR timeseries in this supervised task.

Table 3: **Discriminative score of synthetic data.** A discriminative model is trained post-hoc to discriminate between synthetic samples and real samples. The accuracy from the discriminative classifier is used as the discriminative score, where the lower value indicates better performance. The result is bounded by 0.5 when the classifier cannot distinguish between two distributions.

	Method	MIMIC-III	eICU	HiRID
Continuous-valued synthetic data	C-RNN-GAN	$0.825 \pm 0.013$	$0.876 \pm 0.010$	$0.774 \pm 0.022$
	R(C)GAN	$0.833 \pm 0.028$	$0.850 \pm 0.021$	$0.742 \pm 0.016$
	TimeGAN	$0.763 \pm 0.018$	$0.790 \pm 0.013$	<b><math>0.716 \pm 0.024</math></b>
	$GAN_{VAE}$	$0.842 \pm 0.020$	$0.871 \pm 0.014$	$0.802 \pm 0.017$
	$GAN_{SL}$	$0.786 \pm 0.016$	$0.813 \pm 0.023$	$0.752 \pm 0.021$
	EHR-M-GAN	<b><math>0.746 \pm 0.018</math></b>	<b><math>0.776 \pm 0.015</math></b>	$0.724 \pm 0.015$
Discrete-valued synthetic data	EHR-M-GAN <sub>cond</sub>	<b><math>0.729 \pm 0.025</math></b>	<b><math>0.745 \pm 0.017</math></b>	<b><math>0.693 \pm 0.012</math></b>
	medGAN	$0.903 \pm 0.027$	$0.915 \pm 0.034$	$0.896 \pm 0.021$
	seqGAN	$0.937 \pm 0.025$	$0.924 \pm 0.023$	$0.913 \pm 0.027$
	DualAAE	$0.847 \pm 0.029$	$0.860 \pm 0.033$	$0.829 \pm 0.024$
	$GAN_{VAE}$	$0.862 \pm 0.024$	$0.881 \pm 0.029$	$0.824 \pm 0.018$
	$GAN_{SL}$	$0.829 \pm 0.032$	$0.844 \pm 0.028$	$0.816 \pm 0.025$
	EHR-M-GAN	<b><math>0.813 \pm 0.026</math></b>	<b><math>0.831 \pm 0.024</math></b>	<b><math>0.802 \pm 0.020</math></b>
	EHR-M-GAN <sub>cond</sub>	<b><math>0.784 \pm 0.024</math></b>	<b><math>0.803 \pm 0.022</math></b>	<b><math>0.778 \pm 0.019</math></b>

Results in Table 3 indicate that synthetic data that are highly indistinguishable from the original data are produced by EHR-M-GAN and EHR-M-GAN<sub>cond</sub>. Especially for EHR-M-GAN<sub>cond</sub>, it achieves the optimal discriminative scores consistently against other benchmarks for both continuous-valued and discrete-valued timeseries. For discrete-valued data generation, EHR-M-GAN-generated samples achieve the discriminative score of 0.813 on the MIMIC-III dataset, which is a 4% statistically significant improvement than the best performance among state-of-the-art benchmarks (EHR-M-GAN vs. DualAAE: 0.802 to 0.829,  $p < 0.05$ ). For continuous-valued timeseries generation, the discriminative score of TimeGAN on HiRID dataset outperforms the other models as well as EHR-M-GAN, though not statistically significant (EHR-M-GAN vs. TimeGAN: 0.724 to 0.716,  $p = 0.4374$ ). By leveraging the additional information from the conditional inputs, EHR-M-GAN<sub>cond</sub> can provide significantly better result than TimeGAN (EHR-M-GAN<sub>cond</sub> vs. TimeGAN: 0.693 to 0.716,  $p < 0.05$ ).

The ablation study has proved the effectiveness of EHR-M-GAN for generating high quality EHR timeseries. The shared latent space representation learning in the *dual-VAE* (i.e.,  $GAN_{SL}$ ) have shown remarkable success as making the synthetic data more realistic than separately generating the latent embeddings based on VAEs (as in  $GAN_{VAE}$ ). The *sequentially coupled generator* further improves the model by capturing the dynamics between mixed-type data and iterating over time, therefore enabling the synthetic timeseries to become more indistinguishable from the original.

#### 4.4 PEARSON PAIRWISE CORRELATION

To evaluate the inter- and intra- correlations between continuous-valued and discrete-valued timeseries, we employ Pearson pairwise correlation plot to produce a qualitative comparison between the real

and synthetic data. The positive and negative correlation among each feature pair is measured by Pearson correlation coefficient (PCC), which ranges from -1 to 1.

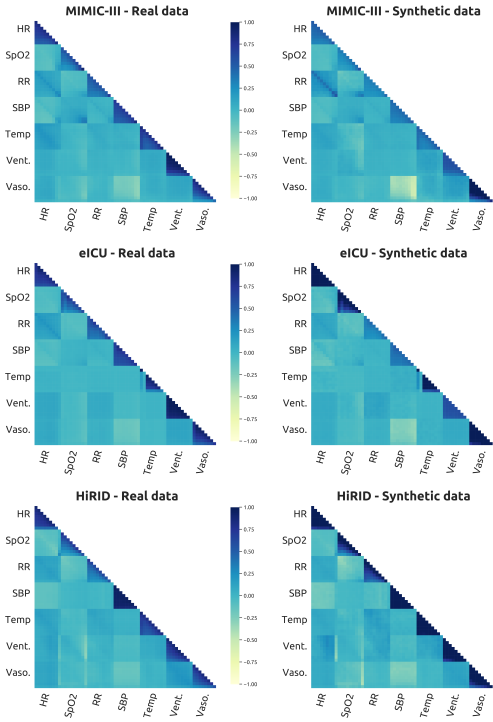


**Figure 3: Pearson pairwise correlation (PPC) between continuous-valued and discrete-valued timeseries.** The plots contrast the PPC calculated within the real data (left column) and the synthetic data generated by EHR-M-GAN (right column).

successfully recover temporal dependencies with a high granularity from real patient trajectories. It is also worth noticing that these three ICU datasets exhibit similar yet not identical correlations over different feature pairs. This demonstrates the data heterogeneity originating from the distribution discrepancy of the underlying patient populations.

#### 4.5 PATIENT TRAJECTORY VISUALISATION

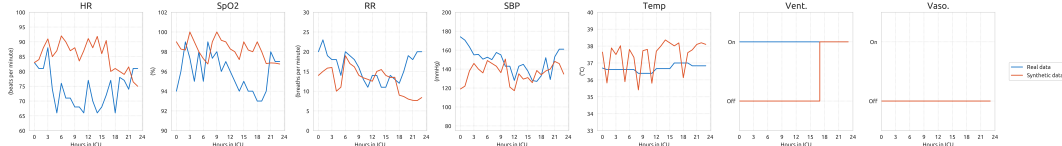
Sample trajectories generated by EHR-M-GAN and EHR-M-GAN<sub>cond</sub> are shown in Fig. 4 for MIMIC-III dataset (see Fig. S6, S7, S8 in Supplementary Materials for more results). By visual inspection, we can see that the proposed models can capture patterns within substantially different time-varying signals. Temporal dynamics in both rapidly fluctuating vital signs (e.g., *Oxygen Saturation*) and infrequently changing intervention (e.g., *Mechanical Ventilation*) can be well-preserved. The variability of the synthetic signals suggests that rather than just intelligently “memorizing” the training data, EHR-M-GAN is capable of modelling the underlying true data distributions in order to produce *genuine* samples.

Furthermore, EHR-M-GAN<sub>cond</sub> shows even more superior performance as it can generate trajectories with predefined patient conditions. From the instance generated by EHR-M-GAN<sub>cond</sub> under the conditional information of *ICU mortality* in Fig. 4, it is possible to observe the variations in physiological signals which suggest that the patient suffers from severe deterioration towards the end of the clinical endpoint. Meanwhile, temporal dependencies are observed within different

Five commonly measured vital sign and laboratory measurement features — *Oxygen Saturation (SpO<sub>2</sub>)*, *Systolic Blood Pressure (SBP)*, *Respiratory Rate (RR)*, *Heart Rate (HR)*, *Temperature (Temp)*, as well as two medical intervention features — *Mechanical Ventilation (Vent.)* and *Vasopressor (Vaso.)* are considered and compared as an exemplar in Fig. 3. Timestamps are extracted with every 3 hours interval in a total of 24 hours ICU stay, to explore the temporal dependencies within different variables (ticks of the timestamps are omitted).

As observed, correlation trends over distinctive features are closely reflected by the synthetic data. For example, negative correlations are shown between *Vasopressor* and *Systolic Blood Pressure* in all three datasets. Similar correlations are also well-captured in the synthetic data provided by EHR-M-GAN. Such correlations can be interpreted as the time-delay effect of prescribing the treatment of vasopressors to elevate mean arterial pressure (MAP) once noticing patients’ abnormal blood pressure.

In addition, temporal dependencies revealed in the original EHR data are also preserved in the synthetic timeseries. For example, synchronized correlations across timestamps are observed between *Respiratory Rate* and *Heart Rate* in MIMIC-III dataset. This can be explained by the common regulation of these two features by the autonomic nervous system and their synchronized increase in cases of physiological stress, such as hypoxemia. Similar trends in the synthetic data suggest that EHR-M-GAN can successfully recover temporal dependencies with a high granularity from real patient trajectories.



(a) Sampled patient trajectories on MIMIC-III dataset using EHR-M-GAN.



(b) Sampled patient trajectories on MIMIC-III dataset using EHR-M-GAN<sub>cond</sub> (under the condition of **ICU mortality**).

**Figure 4: Examples of synthetic patient trajectories.** Multivariate timeseries are generated by EHR-M-GAN and EHR-M-GAN<sub>cond</sub> for the 24 hours before patients' discharge or death in the ICU, including *Oxygen Saturation*, *Systolic Blood Pressure*, *Respiratory Rate*, *Heart Rate*, *Temperature*, *Vasopressor* and *Mechanical Ventilation*. For interventions (vasopressor use and mechanical ventilation), the y-axis indicates whether they are being applied ("On") or not ("Off") at a given time. For the conditional model, EHR-M-GAN<sub>cond</sub>, patient trajectories under 4 conditions — **ICU mortality**, **Hospital mortality**, **30-day readmission**, **No 30-day readmission** — are generated individually (only the condition of *ICU mortality* is shown here). Synthetic patient trajectories under the rest of the conditions in MIMIC-III, and results on eICU and HiRID dataset can be found in Supplementary materials.

physiological signals along with medical intervention. Synchronized correlations are shown between *Oxygen Saturation*, *Systolic Blood Pressure*, and *Heart Rate* from approximately 18 hr to 21 hr, followed by the presence of *Mechanical Ventilation* for providing the respiratory support for the patient at 22 hr.

#### 4.6 EMBEDDING VISUALISATION

Conditional GAN helps to generate patient data with a set of specific medical conditions (Mirza & Osindero, 2014), therefore improving the diversity of the data when synthesizing clinical timeseries. We apply t-SNE to qualitatively visualise the latent embedding generated by EHR-M-GAN<sub>cond</sub>. The distributions of the latent embeddings are induced by the encoders in the *dual-VAE* during learning the shared latent space representations. As shown in Fig. S5, good separability is shown in the latent representations recovered from EHR-M-GAN<sub>cond</sub>. On the other hand, the result also indicates that raw EHR timeseries do not have distinctly different modes in the lower dimensional space. By leveraging the conditional information and placing the semantic loss constraint to learn the shared latent representations, the conditional version of the proposed model can further yield benefits by synthesizing condition-specific EHR timeseries with respect to distinctive patient health status.

#### 4.7 DOWNSTREAM TASKS

As previously discussed, one of the most prominent goals for GANs is to benefit the future downstream analyses in the real clinical application. A relevant question in the ICU is whether specialized medical treatments, such as therapeutic interventions or organ support, are required for critically ill patients during the admission. Accurate predictions on such tasks can help clinicians to provide actionable, in-time interventions in the resource-intensive ICU. Therefore in this section, **clinical intervention prediction** tasks are implemented to evaluate the potential of EHR-M-GAN and EHR-M-GAN<sub>cond</sub> in synthesizing high-fidelity synthetic data to further boost the performance of ML classifiers. In line with prior work (Wang *et al.*, 2020; Wu *et al.*, 2017; Suresh *et al.*, 2017), we establish LSTM-based classifiers to predict the status of *mechanical ventilation* and *vasopressors* using continuous-valued multivariate physiological signals as the predictors. A fixed duration of 12 hours is used for both observation window and prediction window (see Fig. 5). Four outcomes of medical intervention

status are defined as: *Stay on*, *Onset*, *Switch off*, *Stay off* (detailed descriptions can be found in Fig. 5).

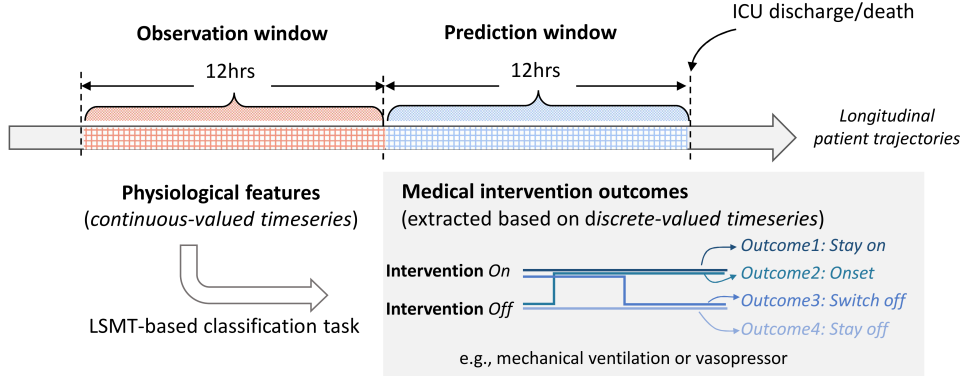


Figure 5: **Downstream prediction example.** Data within 24-hours prior to the patient’s endpoints in the ICU (discharge or mortality) is extracted. Both the observation window and prediction window are fixed as 12 hours. The classification task is to use patients’ continuous-valued physiological measurements within the observation window as input, to predict the forthcoming discrete-valued medical intervention status in the prediction window. The four outcomes of the intervention status can be categorized as follows: ***Stay On***: The intervention begins with *on* and *stays on* within the prediction window; ***Onset***: The intervention begins with *off* and is *turned on* within the prediction window; ***Switch off***: The intervention begins with *on* and is *stopped* within the prediction window; ***Stay Off***: The intervention begins with *off* and *stays off* within the prediction window.

We partition the dataset as illustrated in Figure 6a, and the performances are assessed from two aspects (see Figure 6b): **(i) Traditional approach:** To explore whether the synthetic data can represent the real data accurately, we compare *Train on Real, Test on Real* (TRTR) with *Train on Synthetic, Test on Real* (TSTR), to show whether the performance of a classifier trained on synthetic data from EHR-M-GAN or EHR-M-GAN<sub>cond</sub> can be generalized to real data; and **(ii) Data augmentation approach:** As data augmentation is employed as a means of circumventing the issue caused by the under-resourced EHR data, here we explore whether synthetic data can be used to improve the existing ML algorithms through data augmentation. Therefore, *Train on Synthetic and Real, Test on Real* (TSRTR) is compared with TRTR to measure the improvement of the classifier’s performance when trained on the augmented data (Esteban *et al.*, 2017; Kiyasseh *et al.*, 2020). The augmentation ratio  $\alpha$  or  $\beta$  is applied on sub-train data  $A'_{Tr}$  or synthetic data  $B$ , in two different scenarios of TSRTR, respectively. Details are explained as follows (also see Figure 6b for illustration).

Firstly, as the dearth of data potentially degrades the performance of downstream classifiers, given that the real data has a limited and fixed sample size, we investigate whether adding synthetic EHR data provided by EHR-M-GAN and EHR-M-GAN<sub>cond</sub> can improve the training of downstream classifiers. **Ratio  $\alpha$**  indicates the portion of synthetic data (see Figure 6b) being used to augment the real data to improve the quality and robustness of the downstream classifiers.  $\alpha$  is set to be 10%, 25%, and 50%, representing the availability of synthetic samples provided for augmentation.

Secondly, the acquisition of healthcare data is generally time-consuming and expensive, therefore another overarching goal for the generative model is to minimize the efforts in collecting data. In this section, we investigate whether high-fidelity synthetic data can offer a viable solution for boosting the downstream classifiers’ performance when the availability of real data is limited. This allows us to understand if the sample size required for real data collection can be reduced while maintaining sufficient predictive power through the use of synthetic data. During the experiment, the synthetic data  $B$  is given (to emulate the scenario where synthetic datasets are available for a particular clinical research purpose), which further is combined with limited real data (collected during clinical trial), to train the downstream classifiers (i.e., augment synthetic data with limited real data). Then by implementing EHR-M-GAN or EHR-M-GAN<sub>cond</sub> in TSRTR, we investigate the proportion of the real data  $A'_{Tr}$  (**ratio  $\beta$** ) required to maintain the same performance as in TRTR based on the entire synthetic dataset  $B$  (see Figure 6b).

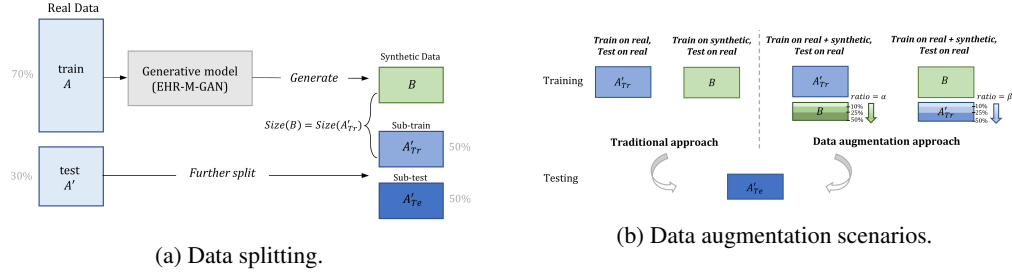


Figure 6: **Downstream intervention prediction experimental setup.** **a. Data splitting.** During training stage, the real data is split into two sets with 70% training data  $A$  and 30% test data  $A'$ . The test data  $A'$  is further split into sub-train data  $A'_{Tr}$  and sub-test data  $A'_{Te}$  with equal size. Then, the synthetic data  $B$ , with size equal to the sub-train data  $A'_{Tr}$ , is synthesized by EHR-M-GAN (or EHR-M-GAN<sub>cond</sub>) trained on the real training data  $A$ . **b. Data augmentation scenarios.** Subsequent experiments are trained on set  $A'_{Tr}$ , or  $B$ , or  $A'_{Tr} \cup B$  and then tested on  $A'_{Te}$ . In traditional approach, results based on *Train on Real, Test on Real (TRTR)* and *Train on Synthetic, Test on Real (TSTR)* are compared to assess the generalisability of the synthetic data. In data augmentation approach, i.e., *Train on Synthetic and Real, Test on Real (TSRTR)*, we either augment real data  $A'_{Tr}$  with  $\alpha$  (augmentation ratio, 0 to 50%) of the synthetic samples  $B$ , or augment synthetic samples  $B$  with  $\beta$  (0 to 50%) of the real data  $A'_{Tr}$ .

**Traditional approach.** Table 4a compares the classification performances of predicting forthcoming medical interventions in the ICUs under the experimental setting of *TRTR* and *TSTR*. It is expected that the optimal AUROCs are achieved by the classifiers that are trained on real data. In comparison, the classifiers trained on the synthetic data provided by proposed models can achieve similar performances. More specifically, synthetic data generated by EHR-M-GAN<sub>cond</sub> demonstrates better generalisability when compared with EHR-M-GAN in the downstream application, such as the task of predicting *mechanical ventilation* on the HiRID dataset (*TRTR* vs. *TSTR* from EHR-M-GAN<sub>cond</sub>: 0.867 to 0.856, with  $p=0.3906$ ).

**Data augmentation approach (with ratio  $\alpha$ ).** The results in Table 4b demonstrate that classifiers boosted by EHR-M-GAN can consistently outperform *TRTR* (see Table 4a) at the augmentation ratio of 50%. In comparison, only 25% of augmentation ratio is needed to achieve improved results for EHR-M-GAN<sub>cond</sub>. For example, the classifier trained on MIMIC-III to predict the status of *Vasopressor* with augmentation ratio  $\alpha$  set as 50%, significantly increase the AUROC by 6% when compared to the classifier trained using only the real data (EHR-M-GAN<sub>cond</sub> vs. *TRTR*: 0.896 to 0.841,  $p < 0.05$ ). Our experiment results have demonstrated that the proposed models can be used for data augmentation to overcome the issue of data scarcity and subsequently improve the classifiers' performance.

**Data augmentation approach (with ratio  $\beta$ ).** On the other hand, as shown in Table 4c, by augmenting with the synthetic data provided by EHR-M-GAN, only approximately 50% of the real data is required to keep the classification AUROCs on par with, or even significantly better than fully exploiting the real data under *TRTR*. For EHR-M-GAN<sub>cond</sub>, the ratio needed for real data to maintain the comparable predictive power is further reduced to 25%, which equivalently indicates a 75% reduction of sample size required in real data collection. Overall, results presented in Table 4c demonstrate that by exploiting only a limited ratio of the real data, EHR-M-GAN and EHR-M-GAN<sub>cond</sub> can robustly maintain the level of prediction performance, therefore alleviating the necessity for acquiring clinical data at scale.

#### 4.8 PRIVACY RISK EVALUATION

Patient privacy is a major concern with regards to sharing electronic health records in any means. Although generative models overcome the explicit one-to-one mapping towards the underlying original data (in contrast to data anonymisation), GAN could potentially raise privacy concerns of information leakage if they simply “memorise” the training data. In that case, sensitive medical information (e.g. national insurance number) belonging to a specific patient used in training GANs can

**Table 4: Downstream task evaluation.** Downstream tasks are evaluated under the training scenarios of *Train on Real, Test on Real (TRTR)*, *Train on Synthetic, Test on Real (TSTR)*, or *Train on Synthetic and Real, Test on Real (TSRTR)*. Prediction of two outcomes of interest – intervention by *Mechanical ventilation (Vent.)* and *Vasopressors (Vaso.)* are selected as exemplary tasks. Macro-AUROC is used to score the performance of the LSTM-based classifiers on the multi-class prediction tasks (labeled as *Stay on, Onset, Switch off, Stay off*).

(a) Performance of the LSTM-based classifier under *TRTR* and *TSTR*.

Dataset	Treatments	Real data	EHR-M-GAN	EHR-M-GAN <sub>cond</sub>
MIMIC-III	Vent.	<b>0.894 ± 0.016</b>	0.740 ± 0.009	0.823 ± 0.020
	Vaso.	<b>0.841 ± 0.009</b>	0.725 ± 0.015	0.810 ± 0.019
eICU	Vent.	<b>0.868 ± 0.015</b>	0.745 ± 0.008	0.795 ± 0.015
	Vaso.	<b>0.813 ± 0.018</b>	0.706 ± 0.014	0.748 ± 0.017
HiRID	Vent.	<b>0.867 ± 0.012</b>	0.825 ± 0.019	0.856 ± 0.033
	Vaso.	<b>0.878 ± 0.010</b>	0.814 ± 0.015	0.844 ± 0.018

(b) Performance of the downstream LSTM-based classifier under *TSRTR* with data augmentation. All data from sub-train data  $A'_{Tr}$  concated with  $\alpha$  of the synthetic data  $B$  (augmentation ratio  $\alpha = 10\%, 25\%$  or  $50\%$ ) is used as the training set. The upper arrow ( $\uparrow$ ) indicates that the AUROC value under *TSRTR* is higher than *TRTR* for the corresponding task, while the bold arrow ( $\uparrow\uparrow$ ) indicates that the value is significantly improved using *t*-test ( $p \leq 0.05$ ).

Dataset	Treatments	EHR-M-GAN			EHR-M-GAN <sub>cond</sub>		
		$\alpha = 10\%$	$\alpha = 25\%$	$\alpha = 50\%$	$\alpha = 10\%$	$\alpha = 25\%$	$\alpha = 50\%$
MIMIC-III	Vent.	0.828 ± 0.013	0.877 ± 0.014	0.912 ± 0.015 ( $\uparrow\uparrow$ )	0.845 ± 0.022	0.896 ± 0.013 ( $\uparrow\uparrow$ )	<b>0.923 ± 0.018 (<math>\uparrow\uparrow</math>)</b>
	Vaso.	0.816 ± 0.015	0.834 ± 0.023	0.859 ± 0.013 ( $\uparrow\uparrow$ )	0.848 ± 0.012 ( $\uparrow$ )	0.876 ± 0.017 ( $\uparrow\uparrow$ )	<b>0.896 ± 0.015 (<math>\uparrow\uparrow</math>)</b>
eICU	Vent.	0.858 ± 0.008	0.862 ± 0.012	0.873 ± 0.014 ( $\uparrow$ )	0.865 ± 0.009	0.879 ± 0.014 ( $\uparrow$ )	<b>0.883 ± 0.016 (<math>\uparrow</math>)</b>
	Vaso.	0.798 ± 0.015	0.805 ± 0.020	0.821 ± 0.028 ( $\uparrow$ )	0.813 ± 0.016 ( $\uparrow$ )	0.834 ± 0.019 ( $\uparrow\uparrow$ )	<b>0.839 ± 0.014 (<math>\uparrow</math>)</b>
HiRID	Vent.	0.871 ± 0.025 ( $\uparrow$ )	0.882 ± 0.021 ( $\uparrow$ )	0.913 ± 0.019 ( $\uparrow\uparrow$ )	0.894 ± 0.015 ( $\uparrow$ )	0.906 ± 0.018 ( $\uparrow\uparrow$ )	<b>0.923 ± 0.021 (<math>\uparrow</math>)</b>
	Vaso.	0.850 ± 0.016	0.874 ± 0.022	0.894 ± 0.018 ( $\uparrow$ )	0.883 ± 0.017 ( $\uparrow$ )	0.908 ± 0.024 ( $\uparrow$ )	<b>0.913 ± 0.019 (<math>\uparrow</math>)</b>

(c) Performance of the downstream LSTM-based classifier under *TSRTR* with data augmentation. All data from synthetic data  $B$  concated with  $\beta$  of the sub-train data  $A'_{Tr}$  (augmentation ratio  $\beta = 10\%, 25\%$  or  $50\%$ ) is used as the training set. The upper arrow ( $\uparrow$ ) indicates that the AUROC value under *TSRTR* is higher than *TRTR* for the corresponding task, while the bold arrow ( $\uparrow\uparrow$ ) indicates that the value is significantly improved using *t*-test ( $p \leq 0.05$ ).

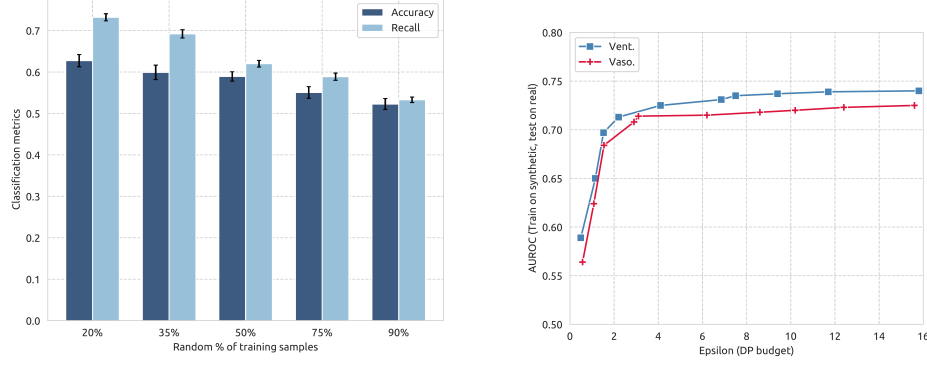
Dataset	Treatments	EHR-M-GAN			EHR-M-GAN <sub>cond</sub>		
		$\beta = 10\%$	$\beta = 25\%$	$\beta = 50\%$	$\beta = 10\%$	$\beta = 25\%$	$\beta = 50\%$
MIMIC-III	Vent.	0.757 ± 0.016	0.824 ± 0.010	0.885 ± 0.009	0.847 ± 0.017	0.903 ± 0.014 ( $\uparrow$ )	<b>0.915 ± 0.009 (<math>\uparrow\uparrow</math>)</b>
	Vaso.	0.786 ± 0.019	0.810 ± 0.020	0.849 ± 0.017 ( $\uparrow$ )	0.823 ± 0.014	0.851 ± 0.019 ( $\uparrow$ )	<b>0.873 ± 0.017 (<math>\uparrow</math>)</b>
eICU	Vent.	0.761 ± 0.011	0.822 ± 0.012	0.870 ± 0.019 ( $\uparrow$ )	0.816 ± 0.016	0.845 ± 0.018	<b>0.872 ± 0.020 (<math>\uparrow</math>)</b>
	Vaso.	0.742 ± 0.014	0.797 ± 0.013	0.846 ± 0.018 ( $\uparrow$ )	0.785 ± 0.022	0.819 ± 0.021 ( $\uparrow$ )	<b>0.834 ± 0.013 (<math>\uparrow</math>)</b>
HiRID	Vent.	0.856 ± 0.012	0.879 ± 0.019 ( $\uparrow$ )	0.895 ± 0.021 ( $\uparrow$ )	0.874 ± 0.016 ( $\uparrow$ )	0.896 ± 0.018 ( $\uparrow\uparrow$ )	<b>0.904 ± 0.012 (<math>\uparrow</math>)</b>
	Vaso.	0.826 ± 0.024	0.859 ± 0.013	0.893 ± 0.018 ( $\uparrow$ )	0.865 ± 0.025	0.897 ± 0.021 ( $\uparrow$ )	<b>0.914 ± 0.018 (<math>\uparrow</math>)</b>

be retrieved during the generative stage, thus posing challenges for preserving privacy in downstream applications.

In this section, we first quantify the vulnerability of EHR-M-GAN to adversary’s **membership inference attacks**, also known as presence disclosure (Hayes *et al.*, 2019; Chen *et al.*, 2020a). The threat model is implemented under the membership inference for GANs in the *black-box settings* (Hayes *et al.*, 2019). The attacker is assumed to possess complete knowledge of all the patient records set  $P$ , where a subset from  $P$  further is used to train GANs. During the experiment, the number of samples in the subset for training EHR-M-GAN are varied to investigate the impact of the availability of training data on the success of the attacker (see Figure 7a). By observing the synthetic patient records from EHR-M-GAN, the adversary’s goal is to determine whether a single known record  $x$  in the patient record set  $P$  is from the data used in training EHR-M-GAN. Determined by whether the attacker can correctly infer a given record is *in* or *not in* GAN’s training, the accuracy and recall can be calculated.

As shown in Figure 7a, when 90% of the training data is used for developing EHR-M-GAN, the attacker had a recall of 0.533 and accuracy of 0.527 to recover which training data are considered. This is eminently close to flipping a coin with random guess (i.e., 0.5), indicating EHR-M-GAN is sufficiently robust against the membership inference attack. On the other hand, as the percentage of the training data reduces, both accuracy and recall for membership inference attacks rise. An accuracy

of 0.624 and recall of 0.732 are reached with 20% of training data. This offers a guideline for future application in developing GANs that incorporating more training data can make the generator less susceptible to such attack. This is also consistent with the conclusion derived from the experiment on membership inference attacks in the prior research (Lin *et al.*, 2020).



(a) Membership inference attack.

(b) Differential privacy.

**Figure 7: Privacy risk evaluation of EHR-M-GAN on MIMIC-III dataset. a. Membership inference attack.** Membership inference attack against EHR-M-GAN vs. the percentage of the training data. Accuracy and recall are used to evaluate the success rate of such attacks. Lower accuracy or recall indicates less privacy information disclosed by the attacker from the generative model (0.5 can be seen as the *random guess* baseline where strong privacy guarantees are provided by GANs). Recall indicates the ratio of samples that are successfully claimed by the attacker among all the real data that are used in training GAN models. **b. Differential privacy.** Performance of medical intervention prediction tasks, under various differential privacy (DP) budgets, measured by Macro-AUROC.

The concept differential privacy (DP) (Dwork, 2008), which appears to be a rigorous mathematical definition of privacy, has emerged to be the prevailing notion in the context of statistically analyzing data privacy. The  $(\epsilon, \delta)$ -differential privacy is guaranteed for model  $M$ , if given any pair of *adjacent* datasets  $D$  and  $D'$  (differing on a single patient record), it holds:  $P[M(D) \in S] \leq e^\epsilon P[M(D') \in S] + \delta$ . In our case,  $M(\cdot)$  is the GAN model trained based on  $D$  or  $D'$ , and  $S$  is the subset of any possible outcomes of the generative process. By perturbing the underlying data distribution, DP bounds the maximum variations of the algorithm when *any* single individual is included or excluded from the dataset. In practice, recent works on developing differentially private deep learning models has benefited from differential private stochastic gradient descent (DP-SGD) algorithm. DP-SGD operates DP by gradient clipping and noise adding during SGD, thereby ensuring that the impact of single record in the training dataset on algorithm parameters is limited within DP's extend. In this section,  $(\epsilon, \delta)$ -differential privacy is implemented in EHR-M-GAN using TensorFlow Privacy<sup>4</sup>. We then perform the same downstream tasks on medical intervention prediction using synthetic data generated from DP-guaranteed EHR-M-GAN, and compare its performance with *TSTR* (as shown in Table 4a).

Figure 7b shows the *TSTR* performance of EHR-M-GAN under differential privacy guarantee with varying budgets  $\epsilon$  ( $\delta$  fixed at  $\leq 0.001$ ). The value  $\epsilon$  determines how strict the privacy is, where the smaller value indicates a stronger privacy restriction. As suggested in Figure 7b, the performance of the downstream tasks operated based on the synthetic data generated by EHR-M-GAN improves as the DP budget relaxes ( $\epsilon$  increases). We observe that the AUROC of DP-bounded EHR-M-GAN can maintain at an acceptable level even under strict privacy setting. For example, the AUROC for predicting the treatment of *Vasopressor* can maintain at 0.714 (AUROC = 0.725 under *TRTR*) even when the  $\epsilon$  decrease to 4, which is an empirically reasonable value for implementing DP in practice (Differential Privacy Team, 2017). Future work that focuses on privacy-preserving GAN under DP-guarantee is expected, where the fidelity of the synthetic data can be restored without compromising its privacy.

<sup>4</sup><https://github.com/tensorflow/privacy>

---

## 5 DISCUSSION AND CONCLUSIONS

In this study, we propose a generative adversarial network entitled EHR-M-GAN, aiming at mitigating the challenge of synthesizing longitudinal EHR with mixed data types. To better capture the correlations between the continuous-valued and discrete-valued timeseries, shared latent representations are learnt based on the proposed *dual-VAE*, where the dimensionality for the subsequent adversarial learning is reduced. Then the proposed *sequentially coupled generator* built based on the architecture of RNNs enables EHR-M-GAN to model the temporal dependencies between heterogeneous data. During the quantitative and qualitative evaluations of the proposed model, both EHR-M-GAN and its conditional version, EHR-M-GAN<sub>cond</sub>, demonstrate consistent improvements against the state-of-the-art benchmark GANs in synthesizing timeseries data with high-fidelity. Notably, as opposed to previous models which were confined to synthesizing only one specific type of data, EHR-M-GAN can produce mixed-type timeseries and successfully capture the temporal dynamics within. During downstream task evaluation, given the prediction of medical interventions in fast-paced critical care environments as an exemplar, the results demonstrate the broad applicability of our model in developing ML algorithm-based decision support tools through data augmentation.

There are limitations in the current work. First, our model is built upon the smoothed timeseries signals, thus making no attempt at modelling the time gaps between signals. As during the data preprocessing, we hourly aggregate patients physiological and medical intervention signals based on their mean statistics, as suggested in MIMIC-Extract (Wang *et al.*, 2020). However, in real clinical data, dealing with irregularity of the timestamps in the sampled physiological timeseries data is still an area of active research, not only for data synthesis, but also for downstream secondary EHR data analysis (Shamout *et al.*, 2019). Modelling such time intervals is non-trivial as the determinative perspectives can sometimes go beyond the scope of inferring patients physiological status, including resource allocations within hospitals, or economic considerations from patients. This could be investigated in future work by incorporating additional inputs from clinical information systems or socioeconomic backgrounds.

Second, although our models successfully extend the scope of synthetic data generation into mixed-type timeseries, they are still limited in single modality (i.e., structured EHR data). However, the adoption of digitized healthcare information systems provide a vast range of other — heterogeneous databases with mixed modalities (Huang *et al.*, 2020). Open-access data with various modalities are provided across the computational health community, including medical image data (such as magnetic resonance imaging (MRI) scans from BraTS (Menze *et al.*, 2014)), physiological waveform signals (such as ECG and PPG data from MIMIC-III Waveform (Moody *et al.*, 2020)), as well as unstructured natural language information (such as free-text clinical notes from i2b2 platform (n2c2., 2021)). Future work can be investigated in the topic of generating synthetic data with multi-modalities, as integrating such data will increase the value of data-driven ML models in the real world clinical applications.

Synthetic data provides an alternative to sharing real patient data while preserving patient privacy. Results in our study demonstrate that the proposed EHR-M-GAN and EHR-M-GAN<sub>cond</sub> can generate realistic longitudinal EHR timeseries with mixed data types. By providing synthetic EHR data with higher fidelity and more variety, the proposed model can therefore enable faster development in AI-driven clinical tools with increased robustness and adaptability. In addition to the improved performance against the existing state-of-the-art benchmark models, augmentation provided by synthetic data during training boosts the predictive performance in downstream clinical tasks. EHR-M-GAN can help eliminate the barriers to data acquisition for healthcare studies, therefore overcoming the challenges posed by the paucity of medical data available and approved for research use.

## REFERENCES

Artzi, Nitzan Shalom, Shilo, Smadar, Hadar, Eran, Rossman, Hagai, Barbash-Hazan, Shiri, Ben-Haroush, Avi, Balicer, Ran D, Feldman, Becca, Wiznitzer, Arnon, & Segal, Eran. 2020. Prediction of gestational diabetes based on nationwide electronic health records. *Nature medicine*, **26**(1), 71–76.

Borji, Ali. 2021. Pros and Cons of GAN Evaluation Measures: New Developments. *arXiv preprint arXiv:2103.09396*.

---

Chen, Dingfan, Yu, Ning, Zhang, Yang, & Fritz, Mario. 2020a. Gan-leaks: A taxonomy of membership inference attacks against generative models. *Pages 343–362 of: Proceedings of the 2020 ACM SIGSAC conference on computer and communications security.*

Chen, Richard J, Lu, Ming Y, Chen, Tiffany Y, Williamson, Drew FK, & Mahmood, Faisal. 2021. Synthetic data in machine learning for medicine and healthcare. *Nature Biomedical Engineering*, 1–5.

Chen, Ting, Kornblith, Simon, Norouzi, Mohammad, & Hinton, Geoffrey. 2020b. A simple framework for contrastive learning of visual representations. *Pages 1597–1607 of: International conference on machine learning.* PMLR.

Choi, Edward, Biswal, Siddharth, Malin, Bradley, Duke, Jon, Stewart, Walter F, & Sun, Jimeng. 2017. Generating multi-label discrete patient records using generative adversarial networks. *Pages 286–305 of: Machine learning for healthcare conference.* PMLR.

CPRD. 2021. *Synthetic data at CPRD.* <https://www.cprd.com/content/synthetic-data>. Accessed: 2021-12-02.

Differential Privacy Team, Apple. 2017. Learning with Privacy at Scale.

Dinov, Ivo D. 2016. Methodological challenges and analytic opportunities for modeling and interpreting Big Healthcare Data. *Gigascience*, 5(1), s13742–016.

Dwork, Cynthia. 2006. Differential privacy. *Pages 1–12 of: International Colloquium on Automata, Languages, and Programming.* Springer.

Dwork, Cynthia. 2008. Differential privacy: A survey of results. *Pages 1–19 of: International conference on theory and applications of models of computation.* Springer.

El Emam, Khaled, Mosquera, Lucy, Jonker, Elizabeth, & Sood, Harpreet. 2021. Evaluating the utility of synthetic COVID-19 case data. *JAMIA open*, 4(1), ooab012.

Esteban, Cristóbal, Hyland, Stephanie L, & Rätsch, Gunnar. 2017. Real-valued (medical) time series generation with recurrent conditional gans. *arXiv preprint arXiv:1706.02633.*

Esteva, Andre, Chou, Katherine, Yeung, Serena, Naik, Nikhil, Madani, Ali, Mottaghi, Ali, Liu, Yun, Topol, Eric, Dean, Jeff, & Socher, Richard. 2021. Deep learning-enabled medical computer vision. *NPJ digital medicine*, 4(1), 1–9.

Frid-Adar, Maayan, Diamant, Idit, Klang, Eyal, Amitai, Michal, Goldberger, Jacob, & Greenspan, Hayit. 2018. GAN-based synthetic medical image augmentation for increased CNN performance in liver lesion classification. *Neurocomputing*, 321, 321–331.

Futoma, Joseph, Simons, Morgan, Panch, Trishan, Doshi-Velez, Finale, & Celi, Leo Anthony. 2020. The myth of generalisability in clinical research and machine learning in health care. *The Lancet Digital Health*, 2(9), e489–e492.

Ghassemi, Marzyeh, Wu, Mike, Hughes, Michael C, Szolovits, Peter, & Doshi-Velez, Finale. 2017. Predicting intervention onset in the ICU with switching state space models. *AMIA Summits on Translational Science Proceedings*, 2017, 82.

Goodfellow, Ian, Pouget-Abadie, Jean, Mirza, Mehdi, Xu, Bing, Warde-Farley, David, Ozair, Sherjil, Courville, Aaron, & Bengio, Yoshua. 2014. Generative adversarial nets. *Advances in neural information processing systems*, 27.

Hayes, Jamie, Melis, Luca, Danezis, George, & De Cristofaro, Emiliano. 2019. Logan: Membership inference attacks against generative models. *Pages 133–152 of: Proceedings on Privacy Enhancing Technologies (PoPETs)*, vol. 2019. De Gruyter.

Huang, Shih-Cheng, Pareek, Anuj, Seyyedi, Saeed, Banerjee, Imon, & Lungren, Matthew P. 2020. Fusion of medical imaging and electronic health records using deep learning: a systematic review and implementation guidelines. *NPJ digital medicine*, 3(1), 1–9.

---

Johnson, Alistair EW, Pollard, Tom J, Shen, Lu, Li-Wei, H Lehman, Feng, Mengling, Ghassemi, Mohammad, Moody, Benjamin, Szolovits, Peter, Celi, Leo Anthony, & Mark, Roger G. 2016. MIMIC-III, a freely accessible critical care database. *Scientific data*, **3**(1), 1–9.

Jordon, James, Yoon, Jinsung, & Van Der Schaar, Mihaela. 2018. PATE-GAN: Generating synthetic data with differential privacy guarantees. In: *International conference on learning representations*.

Jordon, James, Wilson, Alan, & van der Schaar, Mihaela. 2020. Synthetic Data: Opening the data floodgates to enable faster, more directed development of machine learning methods. *arXiv preprint arXiv:2012.04580*.

Kearney, Vasant, Chan, Jason W, Wang, Tianqi, Perry, Alan, Descovich, Martina, Morin, Olivier, Yom, Sue S, & Solberg, Timothy D. 2020. DoseGAN: a generative adversarial network for synthetic dose prediction using attention-gated discrimination and generation. *Scientific reports*, **10**(1), 1–8.

Kim, Jihoon, Neumann, Larissa, Paul, Paulina, Day, Michele E, Aratow, Michael, Bell, Douglas S, Doctor, Jason N, Hinske, Ludwig C, Jiang, Xiaoqian, Kim, Katherine K, et al. 2021. Privacy-protecting, reliable response data discovery using COVID-19 patient observations. *Journal of the American Medical Informatics Association*, **28**(8), 1765–1776.

Kiyassee, Dani, Tadesse, Girmaw Abebe, Thwaites, Louise, Zhu, Tingting, Clifton, David, et al. 2020. Plethaugment: Gan-based ppg augmentation for medical diagnosis in low-resource settings. *IEEE journal of biomedical and health informatics*, **24**(11), 3226–3235.

Kiyassee, Dani, Zhu, Tingting, & Clifton, David A. 2021. CloCS: Contrastive learning of cardiac signals across space, time, and patients. Pages 5606–5615 of: *International Conference on Machine Learning*. PMLR.

Lee, Dongha, Yu, Hwanjo, Jiang, Xiaoqian, Rogith, Deevakar, Gudala, Meghana, Tejani, Mubeen, Zhang, Qiuchen, & Xiong, Li. 2020. Generating sequential electronic health records using dual adversarial autoencoder. *Journal of the American Medical Informatics Association*, **27**(9), 1411–1419.

Lin, Zinan, Jain, Alankar, Wang, Chen, Fanti, Giulia, & Sekar, Vyas. 2020. Using GANs for sharing networked time series data: Challenges, initial promise, and open questions. Pages 464–483 of: *Proceedings of the ACM Internet Measurement Conference*.

Liu, Ming-Yu, & Tuzel, Oncel. 2016. Coupled generative adversarial networks. *Advances in neural information processing systems*, **29**, 469–477.

Liu, Ming-Yu, Breuel, Thomas, & Kautz, Jan. 2017. Unsupervised image-to-image translation networks. Pages 700–708 of: *Advances in neural information processing systems*.

Lombardo, Joseph S, & Moniz, Linda J. 2008. Ta method for generation and distribution. *Johns Hopkins APL Technical Digest*, **27**(4), 356.

Marouf, Mohamed, Machart, Pierre, Bansal, Vikas, Kilian, Christoph, Magruder, Daniel S, Krebs, Christian F, & Bonn, Stefan. 2020. Realistic in silico generation and augmentation of single-cell RNA-seq data using generative adversarial networks. *Nature communications*, **11**(1), 1–12.

McLachlan, Scott, Dube, Kudakwashe, & Gallagher, Thomas. 2016. Using the caremap with health incidents statistics for generating the realistic synthetic electronic healthcare record. Pages 439–448 of: *2016 IEEE International Conference on Healthcare Informatics (ICHI)*. IEEE.

Menger, Vincent, Spruit, Marco, Van Est, Roel, Nap, Eline, & Scheepers, Floor. 2019. Machine learning approach to inpatient violence risk assessment using routinely collected clinical notes in electronic health records. *JAMA network open*, **2**(7), e196709–e196709.

Menze, Bjoern H, Jakab, Andras, Bauer, Stefan, Kalpathy-Cramer, Jayashree, Farahani, Keyvan, Kirby, Justin, Burren, Yuliya, Porz, Nicole, Slotboom, Johannes, Wiest, Roland, et al. 2014. The multimodal brain tumor image segmentation benchmark (BRATS). *IEEE transactions on medical imaging*, **34**(10), 1993–2024.

---

Miotto, Riccardo, Wang, Fei, Wang, Shuang, Jiang, Xiaoqian, & Dudley, Joel T. 2018. Deep learning for healthcare: review, opportunities and challenges. *Briefings in bioinformatics*, **19**(6), 1236–1246.

Mirza, Mehdi, & Osindero, Simon. 2014. Conditional generative adversarial nets. *arXiv preprint arXiv:1411.1784*.

Mogren, Olof. 2016. C-RNN-GAN: Continuous recurrent neural networks with adversarial training. *arXiv preprint arXiv:1611.09904*.

Moody, B, Moody, G, Villarroel, M, Clifford, G, & Silva III, I. 2020. *MIMIC-III Waveform Database (version 1.0)*.

n2c2. 2021. *National NLP Clinical Challenges (n2c2). 2022 n2c2 Shared Task and Workshop*. Boston, MA: Harvard Medical School. <https://n2c2.dbmi.hms.harvard.edu/2022-challenge>. Accessed: 2021-12-08.

N3C. 2021. *N3C. Synthetic Data Workstream*. [https://covid.cd2h.org/N3C\\_synthetic\\_data](https://covid.cd2h.org/N3C_synthetic_data). Accessed: 2021-12-02.

Pollard, Tom J, Johnson, Alistair EW, Raffa, Jesse D, Celi, Leo A, Mark, Roger G, & Badawi, Omar. 2018. The eICU Collaborative Research Database, a freely available multi-center database for critical care research. *Scientific data*, **5**(1), 1–13.

Rajkomar, Alvin, Dean, Jeffrey, & Kohane, Isaac. 2019. Machine learning in medicine. *New England Journal of Medicine*, **380**(14), 1347–1358.

Raket, Lars Lau, Jaskolowski, Jörn, Kinon, Bruce J, Brasen, Jens Christian, Jönsson, Linus, Wehnert, Allan, & Fusar-Poli, Paolo. 2020. Dynamic ElecTronic hEalth reCord deTecTion (DETECT) of individuals at risk of a first episode of psychosis: a case-control development and validation study. *The Lancet Digital Health*, **2**(5), e229–e239.

Sanchez-Pinto, L Nelson, Luo, Yuan, & Churpek, Matthew M. 2018. Big data and data science in critical care. *Chest*, **154**(5), 1239–1248.

Schlegl, Thomas, Seeböck, Philipp, Waldstein, Sebastian M, Langs, Georg, & Schmidt-Erfurth, Ursula. 2019. f-AnoGAN: Fast unsupervised anomaly detection with generative adversarial networks. *Medical image analysis*, **54**, 30–44.

Shamout, Farah E, Zhu, Tingting, Sharma, Pulkit, Watkinson, Peter J, & Clifton, David A. 2019. Deep interpretable early warning system for the detection of clinical deterioration. *IEEE journal of biomedical and health informatics*, **24**(2), 437–446.

Shillan, Duncan, Sterne, Jonathan AC, Champneys, Alan, & Gibbison, Ben. 2019. Use of machine learning to analyse routinely collected intensive care unit data: a systematic review. *Critical care*, **23**(1), 1–11.

Shokri, Reza, Stronati, Marco, Song, Congzheng, & Shmatikov, Vitaly. 2017. Membership inference attacks against machine learning models. *Pages 3–18 of: 2017 IEEE Symposium on Security and Privacy (SP)*. IEEE.

Simon, Gregory E, Shortreed, Susan M, Coley, R Yates, Penfold, Robert B, Rossom, Rebecca C, Waitzfelder, Beth E, Sanchez, Katherine, & Lynch, Frances L. 2019. Assessing and minimizing re-identification risk in research data derived from health care records. *eGEMS*, **7**(1).

Suresh, Harini, Hunt, Nathan, Johnson, Alistair, Celi, Leo Anthony, Szolovits, Peter, & Ghassemi, Marzyeh. 2017. Clinical intervention prediction and understanding with deep neural networks. *Pages 322–337 of: Machine Learning for Healthcare Conference*. PMLR.

Sutherland, Danica J, Tung, Hsiao-Yu, Strathmann, Heiko, De, Soumyajit, Ramdas, Aaditya, Smola, Alex, & Gretton, Arthur. 2016. Generative models and model criticism via optimized maximum mean discrepancy. *arXiv preprint arXiv:1611.04488*.

Tucker, Allan, Wang, Zhenchen, Rotalinti, Ylenia, & Myles, Puja. 2020. Generating high-fidelity synthetic patient data for assessing machine learning healthcare software. *NPJ digital medicine*, **3**(1), 1–13.

---

Wan, Ziyu, Zhang, Bo, Chen, Dongdong, Zhang, Pan, Chen, Dong, Liao, Jing, & Wen, Fang. 2020. Old photo restoration via deep latent space translation. *arXiv preprint arXiv:2009.07047*.

Wang, Lu, Zhang, Wei, & He, Xiaofeng. 2019. Continuous patient-centric sequence generation via sequentially coupled adversarial learning. *Pages 36–52 of: International Conference on Database Systems for Advanced Applications*. Springer.

Wang, Shirly, McDermott, Matthew BA, Chauhan, Geeticka, Ghassemi, Marzyeh, Hughes, Michael C, & Naumann, Tristan. 2020. Mimicextract: A data extraction, preprocessing, and representation pipeline for mimic-iii. *Pages 222–235 of: Proceedings of the ACM Conference on Health, Inference, and Learning*.

Watson, David S, Krutzinna, Jenny, Bruce, Ian N, Griffiths, Christopher EM, McInnes, Iain B, Barnes, Michael R, & Floridi, Luciano. 2019. Clinical applications of machine learning algorithms: beyond the black box. *Bmj*, **364**.

Wilkinson, Jack, Arnold, Kellyn F, Murray, Eleanor J, van Smeden, Maarten, Carr, Kareem, Sippy, Rachel, de Kamps, Marc, Beam, Andrew, Konigorski, Stefan, Lippert, Christoph, *et al.* 2020. Time to reality check the promises of machine learning-powered precision medicine. *The Lancet Digital Health*.

Wirth, Felix Nikolaus, Meurers, Thierry, Johns, Marco, & Prasser, Fabian. 2021. Privacy-preserving data sharing infrastructures for medical research: systematization and comparison. *BMC Medical Informatics and Decision Making*, **21**(1), 1–13.

Wu, Mike, Ghassemi, Marzyeh, Feng, Mengling, Celi, Leo A, Szolovits, Peter, & Doshi-Velez, Finale. 2017. Understanding vasopressor intervention and weaning: risk prediction in a public heterogeneous clinical time series database. *Journal of the American Medical Informatics Association*, **24**(3), 488–495.

Yang, Qingsong, Yan, Pingkun, Zhang, Yanbo, Yu, Hengyong, Shi, Yongyi, Mou, Xuanqin, Kalra, Mannudeep K, Zhang, Yi, Sun, Ling, & Wang, Ge. 2018. Low-dose CT image denoising using a generative adversarial network with Wasserstein distance and perceptual loss. *IEEE transactions on medical imaging*, **37**(6), 1348–1357.

Yèche, Hugo, Kuznetsova, Rita, Zimmermann, Marc, Hüser, Matthias, Lyu, Xinrui, Faltys, Martin, & Ratsch, Gunnar. 2021. HiRID-ICU-Benchmark—A Comprehensive Machine Learning Benchmark on High-resolution ICU Data.

Yoon, Jinsung, Jarrett, Daniel, & Van der Schaar, Mihaela. 2019. Time-series generative adversarial networks.

Yu, Chao, Liu, Jiming, & Zhao, Hongyi. 2019. Inverse reinforcement learning for intelligent mechanical ventilation and sedative dosing in intensive care units. *BMC medical informatics and decision making*, **19**(2), 111–120.

Yu, Lantao, Zhang, Weinan, Wang, Jun, & Yu, Yong. 2017. Seqgan: Sequence generative adversarial nets with policy gradient. *In: Proceedings of the AAAI conference on artificial intelligence*, vol. 31.

Zhang, Ziqi, Yan, Chao, Lasko, Thomas A, Sun, Jimeng, & Malin, Bradley A. 2021. SynTEG: a framework for temporal structured electronic health data simulation. *Journal of the American Medical Informatics Association*, **28**(3), 596–604.

Zhou, Kang, Gao, Shenghua, Cheng, Jun, Gu, Zaiwang, Fu, Huazhu, Tu, Zhi, Yang, Jianlong, Zhao, Yitian, & Liu, Jiang. 2020. Sparse-gan: Sparsity-constrained generative adversarial network for anomaly detection in retinal oct image. *Pages 1227–1231 of: 2020 IEEE 17th International Symposium on Biomedical Imaging (ISBI)*. IEEE.

## 1. METHODOLOGY.

### A. Preliminary of GAN and conditional GAN.

GAN consists of two networks that are adversarially trained to compete against each other. The recurrent neural networks (RNNs) are instantiated considering simulating the temporal structure for generating the sequential data. As shown in Fig. 1 (b. Network architecture) in the main article, the generator  $G$  accepts  $v_{1:T} \in \mathcal{T} \times \mathcal{V}$  as the input, which is a sequence of length  $T$  sampled independently from the a prior distribution [1] (e.g., Gaussian distribution or uniform distribution). Then  $G$  is optimized to approximate the distribution of true data,  $p_x$ , by generating samples  $\hat{x}_{1:T}$  that are hard for the discriminator to distinguish from. Meanwhile, the discriminator  $D$  is optimized to distinguish real samples  $x_{1:T}$  from synthetic samples  $\hat{x}_{1:T}$ . Overall, the training of GAN is a minmax game with the following objective function:

$$\min_G \max_D V_{\text{GAN}} = \mathbb{E}_{x \sim p_x} [\log D(x)] + \mathbb{E}_{v \sim p_v} [\log(1 - D(G(v)))] \quad (\text{S1})$$

Conditional GAN is the extension case of GAN, where both the generator  $G$  and discriminator  $D$  receive conditional information  $y \in \mathcal{L} = \{1, 2, \dots, |L|\}$  from  $|L|$  classes [1]. In other words, the inputs are augmented by being concatenated with  $y$  at each timestamp, i.e.,  $x_{1:T} \rightarrow [y; x_{1:T}]$ . This formulation allows  $G$  to generate samples conditioned on the auxiliary information of  $|L|$ -dimensional categorical labels. In this case, the objective function becomes:

$$\begin{aligned} \min_G \max_D V_{\text{CGAN}} = & \mathbb{E}_{y, x \sim p_{y,x}} [\log D(x|y)] \\ & + \mathbb{E}_{y \sim p_y, v \sim p_v} [\log(1 - D(G(y, v)|y))] \end{aligned} \quad (\text{S2})$$

### B. Shared latent space learning using dual-VAE.

As shown in Fig. S1, the shared latent space is learnt by a dual-VAE network, which contains a pair of encoders (parameterized as  $\phi_{Enc^C}$  and  $\phi_{Enc^D}$ ), and a pair of decoders (parameterized as  $\psi_{Dec^C}$  and  $\psi_{Dec^D}$ ) for mixed-type inputs. The encoders map the observations into the latent space with  $Enc(x) \triangleq q_\phi(z|x)$ , while the decoders further map the representations into the reconstructed input with  $Dec(z) \triangleq p_\psi(x|z)$ . During the implementation, we found that except for pretraining the dual-VAE, integrating the optimization for decoders during the joint training stage also benefit the generative model from learning an improved representations in the shared latent space.

In dual-VAE, we enforce a weight-sharing constraint [2] across certain layers within both the encoders pairs and decoders pairs to further eliminate the gap between domains (see Fig. S1). To be specific, only weights of the last few layers of the encoders and the first few layers of the decoders are shared [3]. This forces the encoders to derive the same high-level representations while maintaining different low-level realizations. Meanwhile, it forces the decoders to share the same high-level semantics and decode them into different low-level feature space observations.

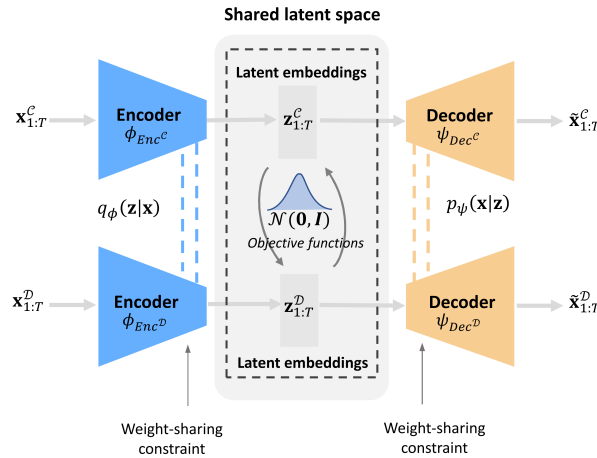


**Fig. S1.** The network architecture of dual-VAE during the pretraining stage.

### C. Single recurrent network (SRN).

The SRN is implemented with Long short-term memory (LSTM) network, which is capable of capturing temporal dynamics among the patient trajectories. Each SRN consists of three layers: (i) At each timestamp  $t \in \{1, 2, \dots, T\}$ , the *input layer* takes the random noise  $v_t$  as the input, which is normally sampled from Gaussian distribution or uniform distribution (e.g.,  $v_t \in \mathcal{U}(0, 1)$ ), and then feed it into the following LSTM network; (ii) The *recurrent layer*  $f_{\text{rec}}$  learns a mapping from  $v_t$  and previous hidden state  $\mathbf{h}_{t-1}$  to  $\mathbf{h}_t$  at current stage, by applying the corresponding transition functions; (iii) At each stage, the output from the LSTM cell is fed into a *fully connected layer*  $f_{\text{conn}}$  with weights shared across timesteps to obtain the generated latent codes  $\hat{\mathbf{z}}_t$ :

$$\begin{aligned} \mathbf{h}_t &= f_{\text{rec}}(\mathbf{v}_t, \mathbf{h}_{t-1}) \\ \hat{\mathbf{z}}_t &= f_{\text{conn}}(\mathbf{h}_t) \end{aligned} \quad (\text{S3})$$

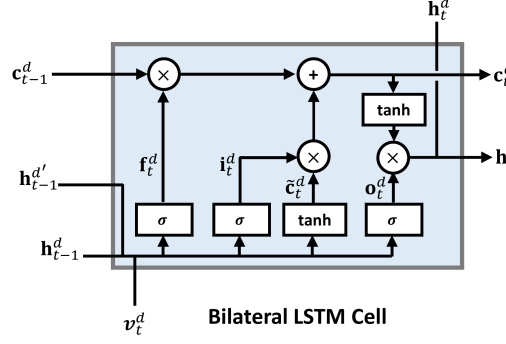


**Fig. S2. Illustration of BLSTM cell.**

The abovementioned steps will recursively process the timeseries with the length of  $T$ . To better compare with BLSTMs, we elaborate the architecture of the LSTM network. LSTM utilizes three gates to control the cell state in order to mitigate the problems of gradient vanishing and exploding that appears in the recurrent neural network (RNN) — an input gate  $\mathbf{i}_t$  that controls the amount of input information to be passed along into the memory cell, a forget gate  $\mathbf{f}_t$  which controls the amount of past information to be neglected, and an output gate  $\mathbf{o}_t$  which controls the update of the new memory cell. The range of outputs from  $\mathbf{i}_t$ ,  $\mathbf{f}_t$  and  $\mathbf{o}_t$  are limited by  $[0, 1]$  due to the sigmoid activation function. At each time step  $t$ , the transition functions in LSTM are as follows:

$$\begin{aligned} \mathbf{i}_t &= \sigma(\mathbf{W}_{iv} \mathbf{v}_t + \mathbf{W}_{ih} \mathbf{h}_{t-1} + \mathbf{b}_i) \\ \mathbf{f}_t &= \sigma(\mathbf{W}_{fv} \mathbf{v}_t + \mathbf{W}_{fh} \mathbf{h}_{t-1} + \mathbf{b}_f) \\ \mathbf{o}_t &= \sigma(\mathbf{W}_{ov} \mathbf{v}_t + \mathbf{W}_{oh} \mathbf{h}_{t-1} + \mathbf{b}_o) \\ \tilde{\mathbf{c}}_t &= \tanh(\mathbf{W}_{cv} \mathbf{v}_t + \mathbf{W}_{ch} \mathbf{h}_{t-1} + \mathbf{b}_c) \\ \mathbf{c}_t &= \mathbf{f}_t \odot \mathbf{c}_{t-1} + \mathbf{i}_t \odot \tilde{\mathbf{c}}_t \\ \mathbf{h}_t &= \mathbf{o}_t \odot \tanh(\mathbf{c}_t) \end{aligned} \quad (\text{S4})$$

where  $\mathbf{c}_t$  denotes the context vector,  $\sigma$  denotes the sigmoid activation function, and  $\odot$  denotes the operation of element-wise multiplication.

Based on the basic structure of LSTM, the Bilateral Long Short-Term Memory (BLSTM) network is proposed (see Fig. S2). Equations that demonstrate the calculation of BLSTM units can be found in *Methodology* section in the main article.

## D. Algorithms.

**Algorithm S1.** Algorithm of dual-VAE for pretraining.

---

1: **Input:**  $\mathcal{D} = \{(\mathbf{x}_{i,1:T}^{\mathcal{C}}, \mathbf{x}_{i,1:T}^{\mathcal{D}})\}_{i=1}^N$ , learning rate  $\eta_{\text{VAE}}$ , scalar loss weights  $\beta_0, \beta_1, \beta_2, \beta_3$  (if conditional), minibatch size  $n_{mb}$ .

2: Initialize parameters:  $\phi_{\text{Enc}}^{\mathcal{C}}, \phi_{\text{Enc}}^{\mathcal{D}}, \psi_{\text{Dec}}^{\mathcal{C}}, \psi_{\text{Dec}}^{\mathcal{D}}$

3: **for** number of pretrain iterations **do**

4:   Sample  $n_{mb}$  minibatches of  $\{(\mathbf{x}_{i,1:T}^{\mathcal{C}}, \mathbf{x}_{i,1:T}^{\mathcal{D}})\}_{i=1}^{n_{mb}}$   $\stackrel{i.i.d.}{\sim} \mathcal{D}$

5:   Map between features and latent representations:

6:   **for**  $i = 1, 2, \dots, n_{mb}, t = 1, 2, \dots, T$  **do**

7:      $(\mathbf{z}_{i,t}^{\mathcal{C}}, \mathbf{z}_{i,t}^{\mathcal{D}}) = (Enc^{\mathcal{C}}(\mathbf{x}_{i,t}^{\mathcal{C}}, \mathbf{z}_{i,t-1}^{\mathcal{C}}), Enc^{\mathcal{D}}(\mathbf{x}_{i,t}^{\mathcal{D}}, \mathbf{z}_{i,t-1}^{\mathcal{D}}))$

8:      $(\tilde{\mathbf{x}}_{i,t}^{\mathcal{C}}, \tilde{\mathbf{x}}_{i,t}^{\mathcal{D}}) = (Dec^{\mathcal{C}}(\mathbf{z}_{i,t}^{\mathcal{C}}), Dec^{\mathcal{D}}(\mathbf{z}_{i,t}^{\mathcal{D}}))$

9:     Estimate the loss terms:

10:    **for**  $d \in \{\mathcal{C}, \mathcal{D}\}$  **do**

11:      $\mathcal{L}_d^{\text{ELBO}} = \frac{1}{n_{mb}} \sum_{i=1}^{n_{mb}} [-\mathbb{E}_{q_{\phi}(\mathbf{z}|\mathbf{x})}[\log p_{\psi}(\mathbf{x}|\mathbf{z})] + \beta_{\text{KL}} D_{\text{KL}}(q_{\phi}(\mathbf{z}|\mathbf{x}) \| p_{\psi}(\mathbf{z}))]$

12:      $\mathcal{L}^{\text{Match}} = \frac{1}{n_{mb}} \sum_{i=1}^{n_{mb}} [\mathbb{E}_{\mathbf{z} \sim p_{\mathbf{z}}} [\sum_{t \in \mathcal{T}} ||\mathbf{z}_t^{\mathcal{C}} - \mathbf{z}_t^{\mathcal{D}}||^2]]$

13:      $\mathcal{L}^{\text{Contra}} = \frac{1}{2n_{mb}} \sum_{i^d=1}^{n_{mb}} \sum_{i^{d'}=1}^{n_{mb}} [\mathcal{L}_{i^d, i^{d'}}^{\text{Contra}} + \mathcal{L}_{i^{d'}, i^d}^{\text{Contra}}]$

14:      $\mathcal{L}_d = \beta_0 \mathcal{L}_d^{\text{ELBO}} + \beta_1 \mathcal{L}^{\text{Match}} + \beta_2 \mathcal{L}^{\text{Contra}}$

15:     **if** conditional **then**

16:        $\mathcal{L}_d^{\text{Class}} = \frac{1}{n_{mb}} \sum_{i=1}^{n_{mb}} [\mathbb{E}_{\mathbf{z}^d \sim \mathcal{H}^{\mathcal{S}}} \text{CE} (f_{\text{linear}}^d(\mathbf{z}^d), \mathbf{y})]$

17:        $\mathcal{L}_d = \beta_0 \mathcal{L}_d^{\text{ELBO}} + \beta_1 \mathcal{L}^{\text{Match}} + \beta_2 \mathcal{L}^{\text{Contra}} + \beta_3 \mathcal{L}_d^{\text{Class}}$

18:      $\phi_{\text{Enc}}^{\mathcal{C}} = \text{Adam} \left( \frac{\partial \mathcal{L}_{\text{VAE}}^{\mathcal{C}}}{\partial \phi_{\text{Enc}}^{\mathcal{C}}}, \eta_{\text{VAE}} \right), \psi_{\text{Dec}}^{\mathcal{C}} = \text{Adam} \left( \frac{\partial \mathcal{L}_{\text{VAE}}^{\mathcal{C}}}{\partial \psi_{\text{Dec}}^{\mathcal{C}}}, \eta_{\text{VAE}} \right)$

19:      $\phi_{\text{Enc}}^{\mathcal{D}} = \text{Adam} \left( \frac{\partial \mathcal{L}_{\text{VAE}}^{\mathcal{D}}}{\partial \phi_{\text{Enc}}^{\mathcal{D}}}, \eta_{\text{VAE}} \right), \psi_{\text{Dec}}^{\mathcal{D}} = \text{Adam} \left( \frac{\partial \mathcal{L}_{\text{VAE}}^{\mathcal{D}}}{\partial \psi_{\text{Dec}}^{\mathcal{D}}}, \eta_{\text{VAE}} \right)$

20: **Return:**  $\psi_{\text{Dec}}^{\mathcal{C}}, \psi_{\text{Dec}}^{\mathcal{D}}$

---

**Algorithm S2.** Algorithm of EHR-M-GAN.

---

1: **Input:**  $\mathcal{D} = \{(\mathbf{x}_{i,1:T}^{\mathcal{C}}, \mathbf{x}_{i,1:T}^{\mathcal{D}})\}_{i=1}^N$ , pretrained decoder in dual-VAE for both domains  $\psi_{\text{Dec}}^{\mathcal{C}}, \psi_{\text{Dec}}^{\mathcal{D}}$ , learning rate  $\eta_{\text{GAN}}$ , minibatch size  $n_{mb}$

2: Initialize parameters:  $\theta_G^{\text{CRN}}, \mu_D^{\mathcal{C}}, \mu_D^{\mathcal{D}}$ .

3: **for** number of training iterations **do**

4:   Sample minibatch  $n_{mb}$  of  $\{(\mathbf{v}_{i,1:T}^{\mathcal{C}}, \mathbf{v}_{i,1:T}^{\mathcal{D}})\}_{i=1}^{n_{mb}} \stackrel{i.i.d.}{\sim} \mathcal{V}$

5:   **for**  $i = 1, 2, \dots, n_{mb}, t = 1, 2, \dots, T$  **do**

6:     Generate synthetic latent codes using coupled-generator:

7:      $(\hat{\mathbf{z}}_{i,t}^{\mathcal{C}}, \hat{\mathbf{z}}_{i,t}^{\mathcal{D}}) = G^{\text{CRN}}((\mathbf{v}_{i,t}^{\mathcal{C}}, \mathbf{v}_{i,t}^{\mathcal{D}}), (\mathbf{h}_{i,t-1}^{\mathcal{C}}, \mathbf{h}_{i,t-1}^{\mathcal{D}}))$

8:     Decode generated latent codes into observational space:

9:      $(\hat{\mathbf{x}}_{i,t}^{\mathcal{C}}, \hat{\mathbf{x}}_{i,t}^{\mathcal{D}}) = (Dec^{\mathcal{C}}(\hat{\mathbf{z}}_{i,t}^{\mathcal{C}}), Dec^{\mathcal{D}}(\hat{\mathbf{z}}_{i,t}^{\mathcal{D}}))$

   Sample  $n_{mb}$  minibatches of  $\{(\mathbf{v}_{i,1:T}^{\mathcal{C}}, \mathbf{v}_{i,1:T}^{\mathcal{D}})\}_{i=1}^{n_{mb}} \stackrel{i.i.d.}{\sim} \mathcal{V}, \{(\hat{\mathbf{x}}_{i,1:T}^{\mathcal{C}}, \hat{\mathbf{x}}_{i,1:T}^{\mathcal{D}})\}_{i=1}^{n_{mb}} \stackrel{i.i.d.}{\sim} \mathcal{D}$

10:   Distinguish real and fake samples using discriminators and estimate loss:

11:    $\mathcal{L}_{\text{GAN}} = \frac{1}{n_{mb}} \sum_{n=1}^{n_{mb}} [\log(D^{\mathcal{C}}(\hat{\mathbf{x}}_n^{\mathcal{C}})) + \log(D^{\mathcal{D}}(\hat{\mathbf{x}}_n^{\mathcal{D}}))] +$

12:      $[\log(1 - D^{\mathcal{C}}(\hat{\mathbf{x}}_n^{\mathcal{C}})) + \log(1 - D^{\mathcal{D}}(\hat{\mathbf{x}}_n^{\mathcal{D}}))]$

13:   Update network weights via Adam optimizer:

14:    $\theta_G^{\text{CRN}} = \text{Adam}\left(\frac{\partial \mathcal{L}_{\text{GAN}}}{\partial \theta_G^{\text{CRN}}}, \eta_{\text{GAN}}\right)$

15:    $\mu_D^{\mathcal{C}} = \text{Adam}\left(\frac{\partial \mathcal{L}_{\text{GAN}}}{\partial \mu_D^{\mathcal{C}}}, \eta_{\text{GAN}}\right), \mu_D^{\mathcal{D}} = \text{Adam}\left(\frac{\partial \mathcal{L}_{\text{GAN}}}{\partial \mu_D^{\mathcal{D}}}, \eta_{\text{GAN}}\right)$

16: *Synthesize M pairs of coupled mixed-types of features for M patients:*

17: Sample  $\{(\mathbf{v}_{i,1:T}^{\mathcal{C}}, \mathbf{v}_{i,1:T}^{\mathcal{D}})\}_{i=1}^M \stackrel{i.i.d.}{\sim} \mathcal{V}$

18: **for**  $i = 1, 2, \dots, M, t = 1, 2, \dots, T$  **do**

19:    $(\hat{\mathbf{z}}_{i,t}^{\mathcal{C}}, \hat{\mathbf{z}}_{i,t}^{\mathcal{D}}) = G^{\text{CRN}}((\mathbf{v}_{i,t}^{\mathcal{C}}, \mathbf{v}_{i,t}^{\mathcal{D}}), (\mathbf{h}_{i,t-1}^{\mathcal{C}}, \mathbf{h}_{i,t-1}^{\mathcal{D}}))$

20:    $(\hat{\mathbf{x}}_{i,t}^{\mathcal{C}}, \hat{\mathbf{x}}_{i,t}^{\mathcal{D}}) = (Dec^{\mathcal{C}}(\hat{\mathbf{z}}_{i,t}^{\mathcal{C}}), Dec^{\mathcal{D}}(\hat{\mathbf{z}}_{i,t}^{\mathcal{D}}))$

21: **Return:**  $\hat{\mathcal{D}} = \{(\hat{\mathbf{x}}_{i,1:T}^{\mathcal{C}}, \hat{\mathbf{x}}_{i,1:T}^{\mathcal{D}})\}_{i=1}^M$

---

## 2. DATASETS.

We construct the pipeline of data preprocessing based on the work of MIMIC-Extract [4]. Three large-scale, publicly available datasets — MIMIC-III, eICU, and HiRID are processed based on the standard pipeline. The complete steps for data preprocessing include:

- Cohort selection: In cohort selection, patients in three ICU databases are selected based on the same predefined criteria (see Section 2.A for details).
- Timeseries features extraction: Then, the timeseries features are extracted based on the lists provided in Section 2.C. Both continuous-valued and discrete-valued features are selected accordingly.
- Unit conversion and outlier filtering: Due to the fact that clinical data is often measured in different units, unit conversion are applied (such as converting Fahrenheit to Celsius for *Temperature*). For outlier filtering, a reasonable physiologically valid range are applied for different measurements (see [4] for details).
- Semantic grouping: Next, semantically similar variables are grouped based on clinical concepts (such as *Heart Rate* is recorded as ItemID 211 in CareVUE EHR systems and ItemID 220045 under MetaVision EHR systems). A clinical taxonomy are used to aggregate features that are semantically equivalent [4].
- Hourly aggregation: Timestamps with different granularity are provided for different in three databases. Time-varying physiological signals such as *Heart Rate* are frequently measured (e.g., most parameters under bedside monitoring are recorded every 2 minutes in HiRID dataset [5]). While other features such as laboratory test results are measured infrequently. Therefore, we hourly aggregate the timeseries further into a uniform hourly bucket.
- Imputation and normalization: Finally, imputation method in Section B are used and normalization are applied to obtain the final result of the data matrix.

### A. Cohort selection criteria.

In line with the previous literature [4, 6], the cohort are selected based on the following criteria: (1) Only the first known ICU admission of the patient is selected. This is because the patients who have multiple ICU admission records typically require specific treatments for life-support intervention; (2) Patient has to be an adult at the time of ICU admission (at least 15); (3) The duration of the patients' ICU stay is at least 12 hours and less than 10 days. This is because the treatment for patients who have longer hours in the ICU stay usually indicates their physiological changes can not be directly linked to the positive effect of the treatment (but compensating for the life support treatment being taken off) [6].

### B. Imputation method.

Missing data is imputed based on the method of *Simple Imputation* [7]. The missing timeseries data is imputed as the last observed value, or individual-specific mean if no previous observation is provided. Else, if there is no observation for the subject, the imputation value is set to the global mean of the entire cohort [4, 7].

### C. Timeseries features extraction.

Features of continuous-valued and discrete-valued timeseries are extracted for three critical care databases based on the following lists (for MIMIC-III dataset, see Table S1, S2; for eICU dataset see Table S3, S4; for HiRID dataset, see Table S5, S6).

**Table S1.** List of vital sign and laboratory test features for MIMIC-III dataset. Features are further extracted based on the preprocessed results of MIMIC-Extract (see Appendix A. Feature set in [4]).

Measurement			
heart rate	respiratory rate	systolic blood pressure	diastolic blood pressure
mean blood pressure	oxygen saturation	temperature	glucose
central venous pressure	hematocrit	potassium	sodium
chloride	pulmonary artery pressure systolic	hemoglobin	ph
creatinine	blood urea nitrogen	bicarbonate	platelets
anion gap	co2 (etco2, pco2, etc.)	partial pressure of carbon dioxide	magnesium
white blood cell count	positive end-expiratory pressure set	calcium	fraction inspired oxygen set
red blood cell count	mean corpuscular hemoglobin concentration	mean corpuscular hemoglobin	mean corpuscular volume
tidal volume observed	partial thromboplastin time	prothrombin time inr	prothrombin time pt
phosphate	phosphorous	peak inspiratory pressure	calcium ionized
respiratory rate set	fraction inspired oxygen	tidal volume set	partial pressure of oxygen
cardiac index	co2	systemic vascular resistance	potassium serum
tidal volume spontaneous	plateau pressure	pulmonary artery pressure mean	cardiac output thermodilution
lactate	lactic acid	bilirubin	aspartate aminotransferase
alanine aminotransferase	alkaline phosphate	positive end-expiratory pressure	albumin
troponin-t	neutrophils	lymphocytes	monocytes
ph urine	fibrinogen	lactate dehydrogenase	basophils
cardiac output flick	creatinine urine	pulmonary capillary wedge pressure	red blood cell count urine
white blood cell count urine	cholesterol	cholesterol hdl	post void residual
cholesterol ldl	chloride urine		

**Table S2.** List of medical intervention features for MIMIC-III dataset, where **Intervention** indicates the name of the feature, **Concept** shows the clinical concept it belongs to, and **Source** is the corresponding chart(s) where the variable is extracted based on. Concepts are extracted based on the official MIMIC-III code repository<sup>1</sup>.

Concept	Intervention	Source
Oxygen therapy	supplemental oxygen mechanical ventilation	chartevents, procedureevents_mv
Vasopressor	adenosine dobutamine dopamine epinephrine isuprel milrinone norepinephrine phenylephrine vasopressin	inputevents_cv, inputevents_mv
Antibiotics	antibiotics	prescriptions
Renal therapy	continuous renal replacement therapy	chartevents
Invasive lines	arterial line central line	procedureevents_mv, chartevents
Colloid bolus	colloid bolus	inputevents_mv, inputevents_cv, chartevents
Crystalloid bolus	crystalloid bolus	inputevents_mv, inputevents_cv

<sup>1</sup><https://github.com/MIT-LCP/mimic-code>

**Table S3.** List of vital sign and laboratory test features for eICU dataset. Features are selected base on the recommendation from Rocheteau et al [8].

Measurement			
Hct	calcium	anion gap	MCH
troponin - I	MCHC	PT	PT - INR
-eos	potassium	-basos	albumin
-polys	lactate	glucose	creatinine
AST (SGOT)	Hgb	MPV	WBC × 1000
ALT (SGPT)	HCO3	MCV	-lymphs
Exhaled MV	RDW	chloride	sodium
bicarbonate	pH	urinary specific gravity	SaO2
Tidal Volume (set)	-monos	Heart Rate	BUN
platelets × 1000	total bilirubin	Exhaled TV (patient)	alkaline phos
Noninvasive BP Diastolic	Noninvasive BP Mean	Noninvasive BP Systolic	Base Excess
paO2	FiO2	Temperature	RBC
PTT	magnesium	RR	SpO2
total protein	paCO2	phosphate	

**Table S4.** List of medical intervention features for eICU dataset, where **Intervention** indicates the name of the feature, **Concept** shows the clinical concept it belongs to, and **Source** is the corresponding chart(s) where the variable is extracted based on. Concepts are extracted based on the official eICU code repository <sup>2</sup>.

Concept	Intervention	Source
Oxygen therapy	supplemental oxygen mechanical ventilation	respiratorycharting, nursecharting, treatment
Vasopressor	dopamine epinephrine norepinephrine phenylephrine vasopressin milrinone dobutamine	infusionDrug
Anesthesia	fentanyl propofol midazolam dexmedetomidine	infusionDrug
Anticoagulants	heparin	infusionDrug
Insulin	insulin	infusionDrug
Antibiotics	antibiotics	medication

<sup>2</sup><https://github.com/MIT-LCP/eicu-code>

**Table S5.** List of vital sign and laboratory test features for HiRID dataset. Features are extracted based on the official HiRID preprocessing codes (meta-variables from [Merging stage 3](#)) [5].

Measurement			
HR	T_Central	ABPs	ABPd
ABPm	NIBPs	NIBPd	NIBPm
PAPm	PAPs	PAPd	CO
SvO2(m)	ZVD	ST1	ST2
ST3	SpO2	ETCO2	RR
OUTurine/h	ICP	Liquor/h	a-BE
a_COHb	a_Hb	a_HCO3-	a_Lac
a_MetHb	a_pH	a_pCO2	a.PO2
a_SO2	K+	Na+	Cl-
Ca2+ ionized	phosphate	Mg_lab	Urea
creatinine	INR	glucose	Hb
MCHC	MCV	platelet count	MCH
C-reactive protein	total white blood cell count		

<sup>3</sup><https://github.com/ratschlab/HiRID-ICU-Benchmark>

**Table S6.** List of medical intervention features for HiRID dataset, where **Intervention** indicates the name of the feature, **Concept** shows the clinical concept it belongs to, and **Source** is the corresponding feature names in the official HiRID preprocessing codes (meta-variables from Merging stage <sup>4</sup>) [5] that we extracted based on.

Concept	Intervention	Source
Oxygen therapy	supplemental oxygen	vm23
	mechanical ventilation	vm60
Crystalloids	crystalloids	vm33
Colloids	colloids	vm34
Renal therapy	haemofiltration	vm72
Blood transfusion	packed red blood cells	pm35
	FFP	pm36
	platelets	pm37
Vaspressor/inotropes	norepinephrine	pm39
	epinephrine	pm40
	dobutamine	pm41
	milrinone	pm42
	levosimendan	pm43
	theophyllin	pm44
	vasopressin	pm45
	desmopressin	pm46
Vasodilators	vasodilators	pm47
Antihypertensives	ACE inhibitors	pm48
	Calcium channel blockers	pm50
	Beta-blocker	pm51
Antiarrhythmics	adenosine	pm53
	digoxin	pm54
	amiodarone	pm55
	atropine	pm56
Antibiotics	antibiotics	pm73
	antimycotic	pm74
	antiviral	pm75
Insulin	insulin	pm82, pm83
Pain killers	opioid	pm86
	non-opioid	pm87
Steroids	steroids	pm91
Anticoagulants	heparin	pm95

<sup>4</sup><https://github.com/ratschlab/HiRID-ICU-Benchmark>

### 3. RESULTS.

#### A. Dimensional-wise probability.

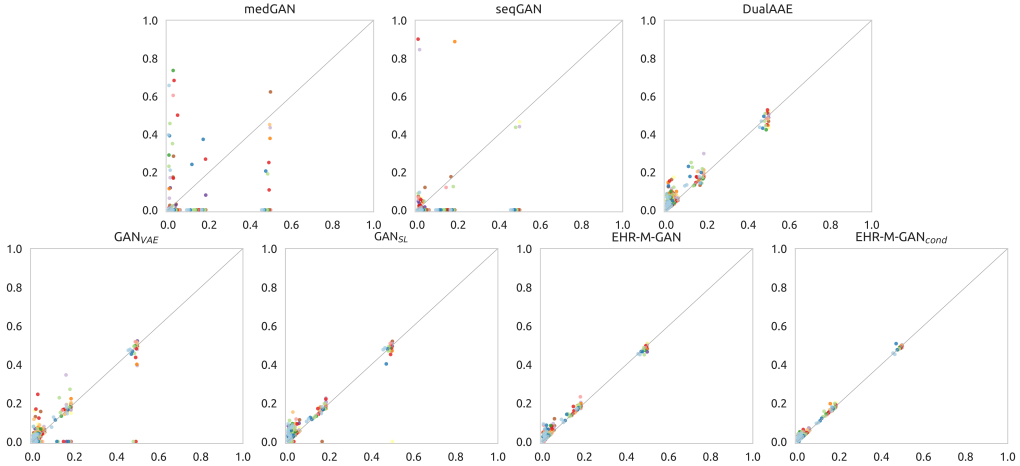


**Fig. S3. Scatterplot of the dimension-wise probability test on eICU dataset.** The x-axis and y-axis represents the probability distribution for the real data and synthetic data with same sample size, respectively. Each dot represents a physiological measurement or treatment status at a particular time in the patient EHR data. Same color indicates same measurement or status (but with varying timestamps). The optimal performance appears along the diagonal line.

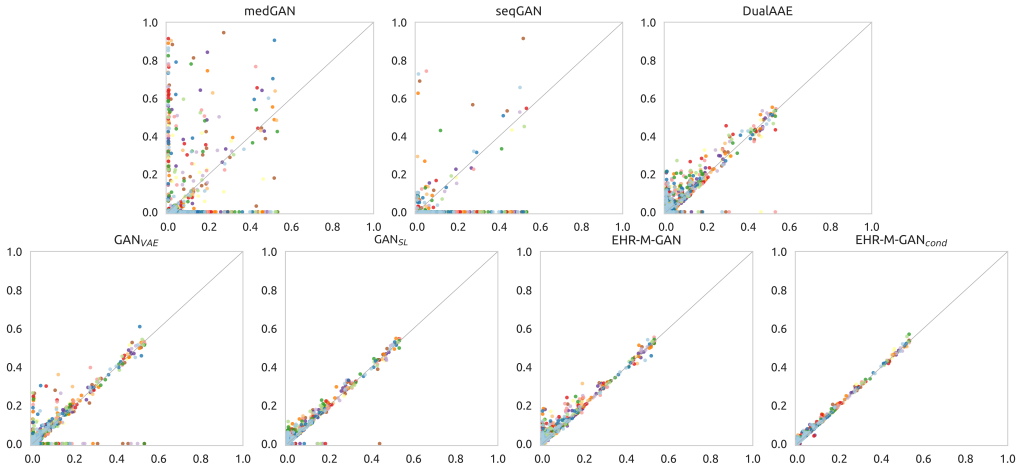


**Fig. S4. Scatterplot of the dimension-wise probability test on HiRID dataset.** The x-axis and y-axis represents the probability distribution for the real data and synthetic data with same sample size, respectively. Each dot represents a physiological measurement or treatment status at a particular time in the patient EHR data. Same color indicates same measurement or status (but with varying timestamps). The optimal performance appears along the diagonal line.

## B. Embedding visualisation.

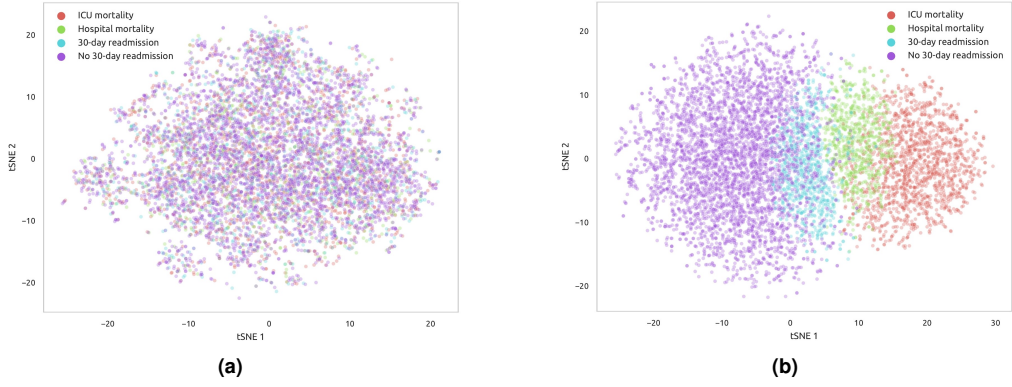
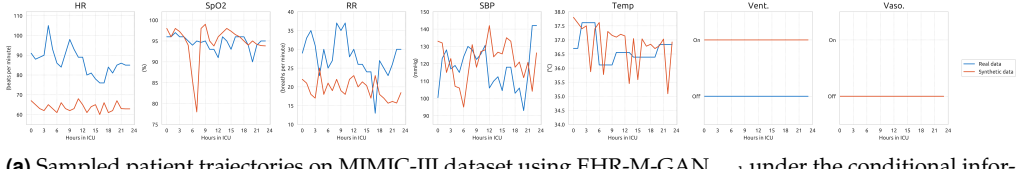
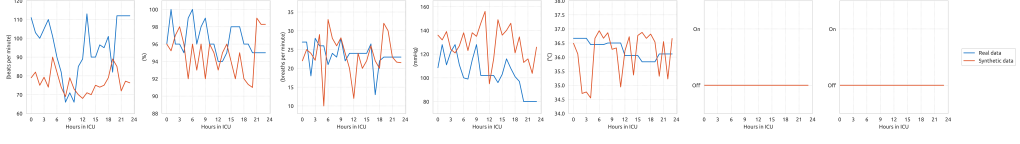


**Fig. S5. Visualization on the latent space embeddings**, using t-SNE on MIMIC-III dataset of (a) raw patient trajectories, and (b) latent embeddings generated with EHR-M-GAN<sub>cond</sub>. Better separability of the representation clusters in the shared latent space are shown in the embeddings obtained from EHR-M-GAN<sub>cond</sub> compared with raw data.

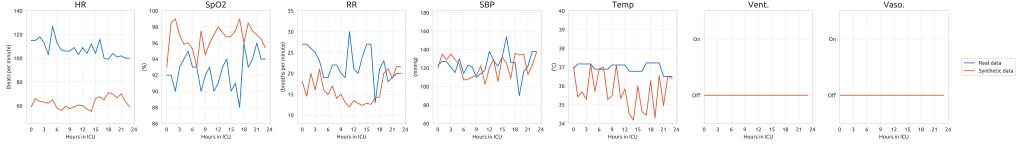
## C. Patient trajectories visualisation.



**(a)** Sampled patient trajectories on MIMIC-III dataset using EHR-M-GAN<sub>cond</sub> under the conditional information of patient status Hospital mortality.

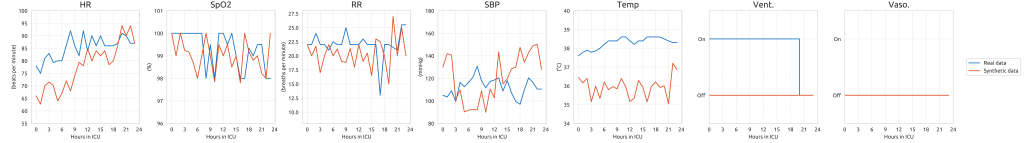


**(b)** Sampled patient trajectories on MIMIC-III dataset using EHR-M-GAN<sub>cond</sub> under the conditional information of patient status 30-day readmission.

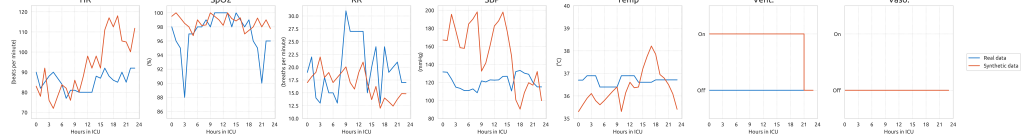


**(c)** Sampled patient trajectories on MIMIC-III dataset using EHR-M-GAN<sub>cond</sub> under the conditional information of patient status No 30-day readmission.

**Fig. S6. Synthetic patient trajectories visualisation for MIMIC-III dataset.** Timeseries are generated by EHR-M-GAN<sub>cond</sub>, within 24 hours before patients being discharged from ICU on specified features, including *Oxygen Saturation*, *Systolic Blood Pressure*, *Respiratory Rate*, *Heart Rate*, *Temperature*, *Vasopressor* and *Mechanical Ventilation*. The binary value of intervention signs indicates whether such medical intervention are put into use.



**(a)** Sampled patient trajectories on eICU dataset using EHR-M-GAN.



**(b)** Sampled patient trajectories on eICU dataset using EHR-M-GAN<sub>cond</sub> under the conditional information of patient status **ICU mortality**.

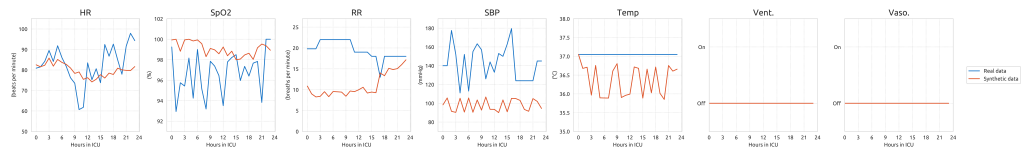


**(c)** Sampled patient trajectories on eICU dataset using EHR-M-GAN<sub>cond</sub> under the conditional information of patient status **Hospital mortality**.

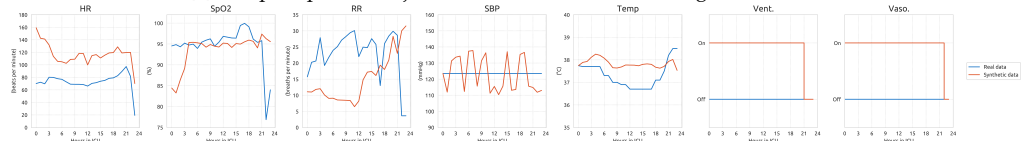


**(d)** Sampled patient trajectories on eICU dataset using EHR-M-GAN<sub>cond</sub> under the conditional information of patient status **Hospital discharge**.

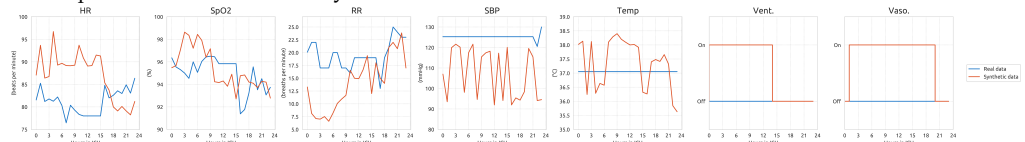
**Fig. S7.** Synthetic patient trajectories visualisation for eICU dataset. Notations can be referred in the caption of Fig. S6.



**(a)** Sampled patient trajectories on HiRID dataset using EHR-M-GAN



**(b)** Sampled patient trajectories on HiRID dataset using EHR-M-GAN<sub>cond</sub> under the conditional information of patient status **ICU mortality**.



**(c)** Sampled patient trajectories on HiRID dataset using EHR-M-GAN<sub>cond</sub> under the conditional information of patient status **ICU discharge**.

**Fig. S8.** Synthetic patient trajectories visualisation for HiRID dataset. Notations can be referred in the caption in Fig. S6.

## REFERENCES

1. Cristóbal Esteban, Stephanie L Hyland, and Gunnar Rätsch. Real-valued (medical) time series generation with recurrent conditional gans. *arXiv preprint arXiv:1706.02633*, 2017.
2. Ming-Yu Liu, Thomas Breuel, and Jan Kautz. Unsupervised image-to-image translation networks. In *Advances in neural information processing systems*, pages 700–708, 2017.
3. Ming-Yu Liu and Oncel Tuzel. Coupled generative adversarial networks. *Advances in neural information processing systems*, 29:469–477, 2016.
4. Shirly Wang, Matthew BA McDermott, Geeticka Chauhan, Marzyeh Ghassemi, Michael C Hughes, and Tristan Naumann. Mimic-extract: A data extraction, preprocessing, and representation pipeline for mimic-iii. In *Proceedings of the ACM Conference on Health, Inference, and Learning*, pages 222–235, 2020.
5. Hugo Yèche, Rita Kuznetsova, Marc Zimmermann, Matthias Hüser, Xinrui Lyu, Martin Faltyš, and Gunnar Rätsch. Hirid-icu-benchmark—a comprehensive machine learning benchmark on high-resolution icu data. 2021.
6. Mike Wu, Marzyeh Ghassemi, Mengling Feng, Leo A Celi, Peter Szolovits, and Finale Doshi-Velez. Understanding vasopressor intervention and weaning: risk prediction in a public heterogeneous clinical time series database. *Journal of the American Medical Informatics Association*, 24(3):488–495, 2017.
7. Zhengping Che, Sanjay Purushotham, Kyunghyun Cho, David Sontag, and Yan Liu. Recurrent neural networks for multivariate time series with missing values. *Scientific reports*, 8(1):1–12, 2018.
8. Emma Rocheteau, Pietro Liò, and Stephanie Hyland. Temporal pointwise convolutional networks for length of stay prediction in the intensive care unit. In *Proceedings of the Conference on Health, Inference, and Learning*, pages 58–68, 2021.